Hydrocarbon Production and Potential
of the Distal Frio Formation,
Texas Coastal Zone and Shelf

BUREAU OF ECONOMIC GEOLOGY

THE UNIVERSITY OF TEXAS
AT AUSTIN
W. L. FISHER, DIRECTOR

Hydrocarbon Production and Potential of the Distal Frio Formation, Texas Coastal Zone and Shelf

by

H. Scott Hamlin

Contract report for Minerals Management Service
under agreement no. 14-12-0001-30296

Bureau of Economic Geology
W. L. Fisher, Director
The University of Texas at Austin
University Station, P. O. Box X
Austin, Texas 78713-7508

1987

CONTENTS

Figures

Tables

Plates (in pocket)

ABSTRACT

The distal Frio Formation along the Texas Coastal Zone and offshore has yielded 680.85 million barrels of oil and 6.54 trillion ft^3 of gas from 153 fields that range in size from 1 to 140 million barrels of oil equivalent. To evaluate the exploration potential of the distal Frio extending deep beneath the Federal Outer Continental Shelf, petroleum production data, regional reservoir-quality and temperature/pressure conditions, and characterization of typical fields were integrated with Galloway's (1986) description of stratigraphy, depositional systems, and structural framework.

The most prospective locations for distal Frio exploration are in the Mustang Island and northeastern Galveston offshore areas, extending as far as 15 mi (24 km) seaward of the 3-league line (Outer Continental Shelf boundary). The North Padre Island offshore area has moderate exploration potential. Significant new discoveries will be deep (9,000 to 16,000 ft [2,740 to 4,880 m]), high-pressure, dry-gas-dominated reservoirs in thin, distal deltaic, strike-reworked delta-margin and distal shoreface/shelf sandstones that will potentially yield 1 to 100 billion ft^3 of gas annually for as long as 10 years.

INTRODUCTION

In the Texas offshore area, the distal margin of the sand-bearing Frio Formation (fig. 1) is a deep, underexplored (relative to onshore Frio) petroleum province. In this report reservoir and production characteristics of the distal Frio beneath the lower coastal plain and offshore State waters are described, and the potential for extending production into the Federal Outer Continental Shelf (OCS) is evaluated. Galloway (1986) extended earlier regional Frio investigations (Galloway and others, 1982) with new well data (pl. 1 and app. A) to better define the deep stratigraphy, structure, and general hydrocarbon potential of the distal Frio. Galloway (1986) mapped sandstone distribution, lithofacies and depositional systems, and regional structural elements and also constructed several dip cross sections. These maps (pls. 2 and 3) and cross sections (pl. 4) are included in this report. Petroleum production maps were constructed for this study to show distal Frio oil and gas fields (pl. 5) and field sizes (pl. 6). Production data were tabulated, graphed, and analyzed statistically. Reservoir-quality trends and temperature/pressure regimes are regionally delineated. Three groups of fields in different distal Frio hydrocarbon plays are used as examples of potential new-field discoveries offshore. Production, reservoir-quality, temperature/pressure, and field-characterization analyses are integrated with the structural, stratigraphic, and facies framework (Galloway, 1986) to outline and qualify optimal fairways for distal Frio exploration in State offshore and Federal OCS areas.

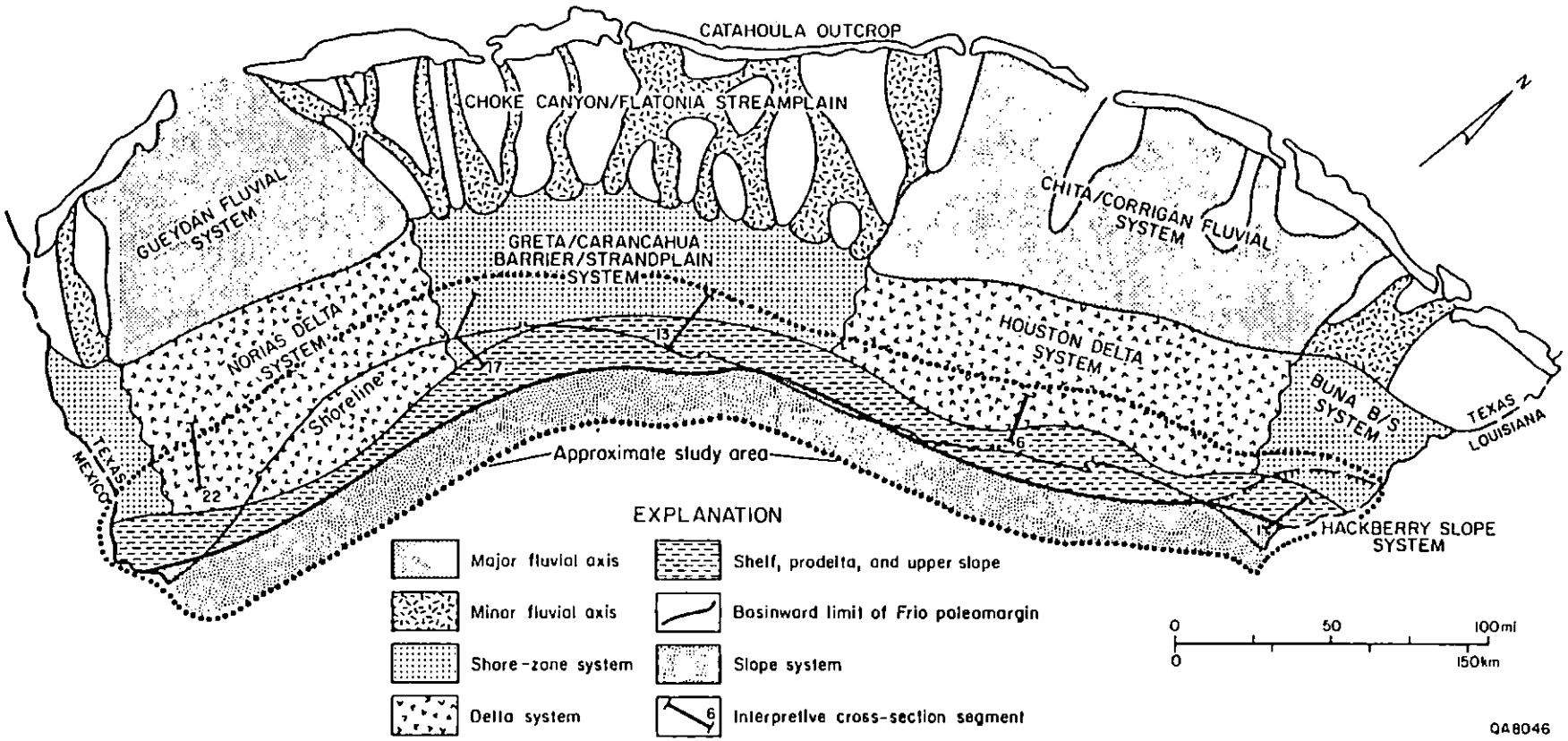

Figure 1. Generalized Frio depositional systems and location of distal Frio study area. Cross sections shown in plate 4. Figure modified from Galloway (1986).

SUMMARY OF RESULTS

1. Major distal Frio hydrocarbon plays produce from reservoirs in barrier/strandplain and deltaic depositional systems.

2. Onshore distal Frio hydrocarbon production has been greatest adjacent to Mustang Island and Galveston offshore areas. Offshore Frio fields are concentrated in State-owned waters in Mustang Island and northeastern Galveston Areas.

3. Most distal Frio fields are small and gas prone.

4. Onshore distal Frio production and discovery trends generally peaked in the 1960's, whereas offshore trends peaked in the late 1970's and early 1980's.

5. Regional porosity trends and studies of typical distal Frio fields indicate that reservoir quality is best developed in (a) delta-front, strike-reworked delta-margin, distal shoreface/shelf, and transgressive sandstones; (b) the shallower parts of the geopressured zone; and (c) Mustang Island and northeastern Galveston offshore and adjacent onshore areas.

6. New Frio discoveries offshore will probably be deep, dry-gas-dominated, short-lived fields. Smaller discoveries will outnumber larger ones.

HYDROCARBON PRODUCTION

By the end of 1985, the distal Frio Formation had produced 680.85 million barrels (bbl) of oil and 6.54 trillion ft^3 (Tcf) of gas, totaling 1.77 billion bbl of oil equivalent (boe) (1 boe = 6,000 ft^3 [6 Mcf] gas). This amount is approximately 11 percent of the more than 16.3 billion boe produced by the entire Frio Formation (Galloway and others, 1982). Large, older onshore fields

historically have accounted for most distal Frio production, but younger fields and new discoveries along the shoreline and offshore are becoming increasingly significant producers. In this section, geographic and temporal distributions of discovery and production are described and related to geologically defined hydrocarbon plays.

Distal Frio Hydrocarbon Plays

Regional Frio hydrocarbon plays I, V, VIII, and IX (Galloway and others, 1982) have been extended into the distal Frio, and several new plays, Va and Xa, have been developed (Galloway, unpublished work maps). Characteristics of distal Frio plays are briefly reviewed here to provide a geologic framework for understanding trends in hydrocarbon production and reservoir conditions.

Distal **play I** (pl. 5) produces from the **Norias delta system** (pl. 2b), the main depocenter in the northwestern Gulf of Mexico during the Oligocene Epoch. Thick deltaic sandstones occur beneath State and Federal waters in the Padre Island and Mustang Island offshore areas (pl. 3). Growth faults and shale ridges are the dominant structures (pl. 2a). Reservoir quality (permeability and porosity) may be reduced diagenetically (Loucks and others, 1984, 1986).

Distal **play V** (pl. 5) produces from the **Greta/Carancahua barrier/strandplain system** along the middle Texas coast (pl. 2b), which includes strike-aligned barrier-core and shoreface/shelf sandstones (Galloway, 1986). In the offshore area, sandstone is best developed in this system adjacent to major deltaic lobes of the Norias delta system (pl. 3). Growth faults and shale ridges are also the dominant structures in this play. Based on production trends (pls. 5 and 6), reservoir quality is better in play V than it is to the south in play I.

Play Va is located in a gas-prone offshore area (pl. 5) on the northern margin of the Norias delta system. It is actually a downdip extension of play V, although play Va reservoirs are typically smaller and deeper. Play Va includes distal, strike-parallel shoreface/shelf sandstones as well as sandstones that may have been transported along the shelf from nearby Norias deltaic headlands and deposited well seaward of the main Greta/Carancahua shore zone (pl. 2b).

Distal parts of **plays VIII and IX** are in the **Houston delta system** along the upper Texas coast (pl. 2b). Only a small part of **play VIII**, which is defined by extensive shallow salt diapirism, occurs along the coast (pl. 5); this is an insignificant distal Frio play. **Play IX** is a major distal play (pl. 5) developed mainly in middle and lower Frio deltaic sandstones along the coast in Brazoria, Galveston, and Chambers Counties (pl. 3). Thinner, distal delta-front and upper-slope sandstones in the Galveston and Brazos offshore areas are proving to be gas productive. Growth faulting and deep-seated salt diapirism are the major structural elements in play IX (pl. 2a). Production trends indicate that good-quality reservoirs are abundant (pls. 5 and 6).

Although located onshore, **play Xa** (pl. 5) is composed of distal facies: reservoirs are deep-water sandstones of the middle Frio **Hackberry slope system**. Play Xa is genetically related to proximal Frio play X (Buna barrier/strandplain system of Galloway and others [1982]). Sand transported along the Buna shoreline was diverted basinward into headwardly eroding Hackberry submarine canyons (Galloway, 1986). As in play IX, growth faulting and salt diapirism dominate structure. Reservoir quality is variable, owing to the complex geometries of the canyon-fill and submarine fan sand bodies (Ewing and Reed, 1984). No Hackberry production occurs offshore.

Production Data and Statistics

Discovery and production trends can be used to project future exploration potential. Cumulative productions and average field sizes are listed by play for the entire distal Frio Formation in table 1. Plays IX and V account for the majority of production and encompass most of the fields. Mean field sizes are skewed toward higher values by a few large fields; mode and median field sizes are generally lower. Cumulative production and annual production for 1985 of individual distal Frio fields are listed in appendix B, but only fields that have produced at least 1 million boe are included. These fields as well as very small fields (<1 million boe) are shown on the petroleum production maps (pls. 5 and 6) and listed in appendix C. A series of graphs based on field production data given in appendix B were also produced for this report. The graph of **cumulative Frio production** (fig. 2), for example, displays data listed in table 1. Of the two largest plays, V is gas prone and IX is oil prone.

Graphs of **field-size distribution** (figs. 3a and 4) show percentages of total distal Frio oil and gas production as well as field frequency (percent of all fields) in field-size categories, which increase exponentially. As is typical of most hydrocarbon-producing areas (Galloway and others, 1982), the greatest percentage of total produced hydrocarbons comes from the largest fields, and yet most fields are small. For all distal Frio plays (fig. 3a), 60 percent of total oil production (>400 million bbl) has been from the 13 largest fields (>32 million boe each). The single largest oil field, Oyster Bayou (play IX), accounts for about 20 percent of total oil production. Gas production is distributed over a larger number of fields and field-size ranges; less than 40 percent of all gas production (about 2.5 Tcf) has come from the 13 largest fields. Almost half of all oil and gas fields have cumulative productions less than 4 million boe, and almost three-

Table 1. Cumulative hydrocarbon production and mean field sizes, distal Frio Formation.

		Cumulative Production			Mean Field Production		
Play	Number of Fields[1]	Oil (MMbbl)[2]	Gas (Bcf)[3]	Total (MMboe)[4]	Oil (MMbbl)	Gas (Bcf)	Total (MMboe)
I	12	34.9	657.1	144.4	2.9	54.8	12.0
V	68	196.7	2,571.2	626.1	2.9	37.8	9.2
Va	5	1.8	284.0	49.1	0.4	56.8	9.8
VIII		4	1.4	172.7	30.2	0.3	43.2
IX	50	404.9	1,859.5	714.8	8.1	37.2	14.3
Xa	14	41.2	999.6	207.8	2.9	71.4	14.8
Total	153	680.9	6,544.0	1,772.4	4.5	42.8	11.6

[1]fields having produced >1 million boe
[2]million barrels
[3]billion cubic feet
[4]million barrels of oil equivalent, where 6 Mcf of gas = 1 boe

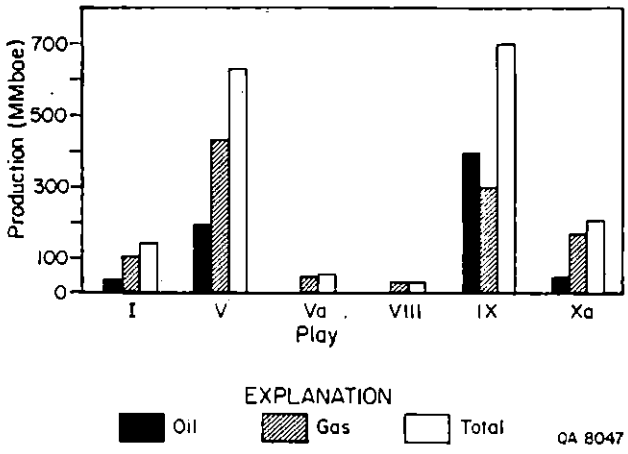

Figure 2. Cumulative production through 1985 from distal Frio Formation by play.

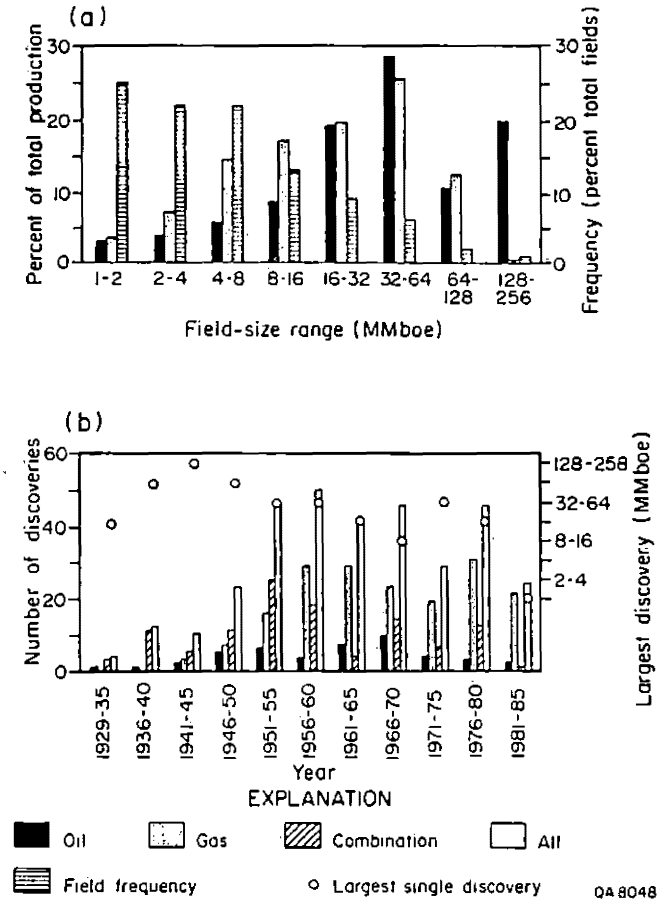

Figure 3. Plots of distal Frio (a) field-size distribution and (b) new-field discovery history.

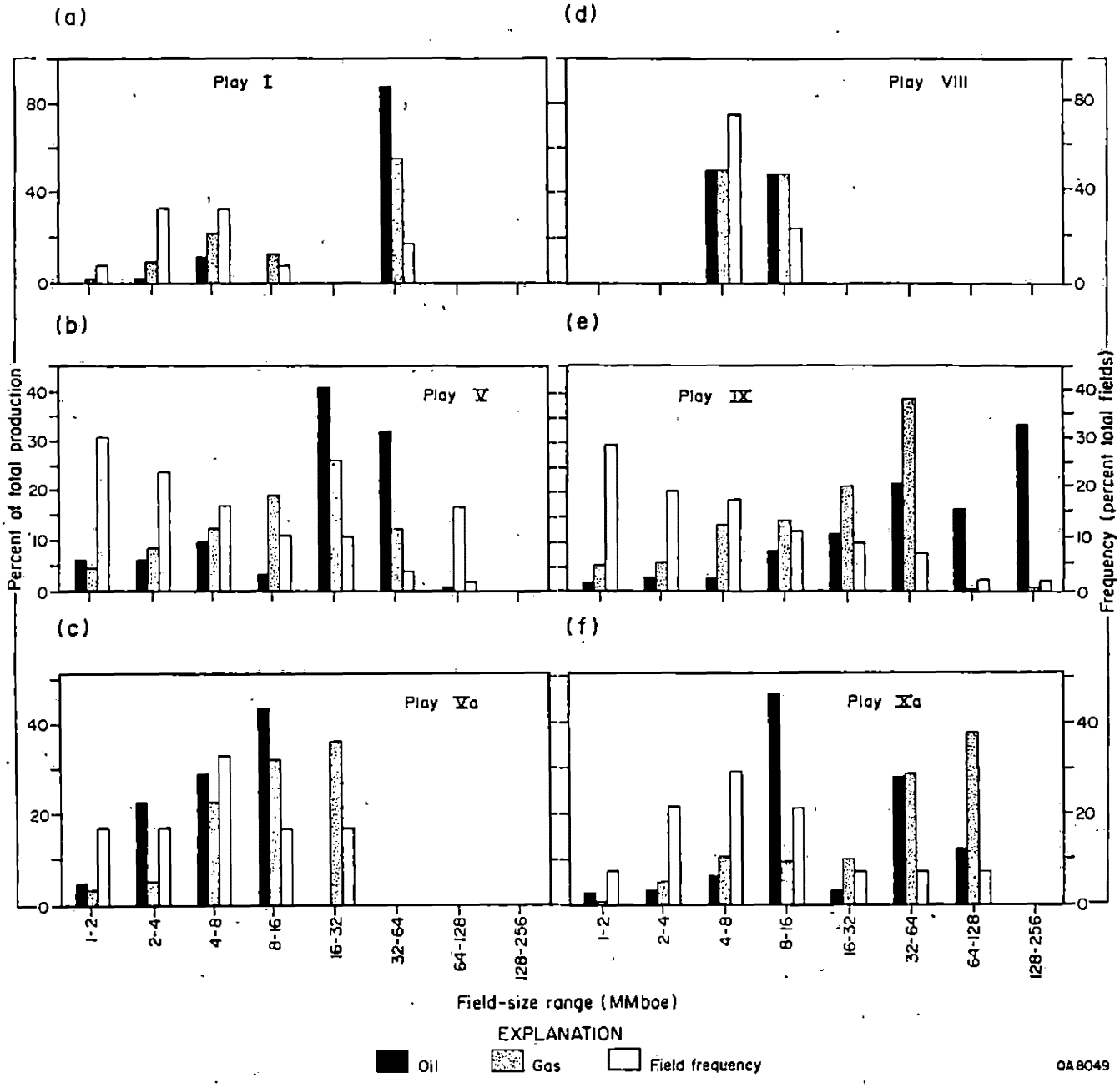

Figure 4. Plots of distal Frio field-size distribution by play.

quarters have produced less than 8 million boe. Graphs of field-size distribution for individual plays (fig. 4) generally show similar patterns, especially in the more productive plays.

Graphs depicting the **new-field discovery history** (figs. 3b and 5) show the number of distal Frio fields discovered in 5-year intervals as well as the size of the largest field discovered in each time interval. For all the distal Frio plays (fig. 3b), about 50 fields have been discovered every 5 years since 1950, except for the periods 1971-1975 (30 fields) and 1981-1985 (about 25 fields). Prior to 1950, few distal Frio fields were discovered. Although most of the largest (>64 million boe) distal Frio fields were discovered early (before 1950), the largest-field discovery trend did not decline dramatically until after 1980 (fig. 3b). Post-1980 fields have not produced long enough to generate high cumulative productions, although a few may have that potential. Graphs of the new-field discovery history show that, in general, the distal Frio is a less mature petroleum exploration trend than the more updip and shallower proximal Frio trend. Most offshore Mustang Island area Frio fields (play Va, fig. 5c) have been discovered since 1980.

Graphs of **annual production histories** (1969 to 1985) for onshore and offshore distal Frio fields appear in figure 6. A group of large (>10 million boe) fields in State-owned submerged lands (bays and lagoons) was selected as a representative sample for tracing onshore production trends (fig. 6a). These 20 fields are the major Frio discoveries along the downdip fringe of the mature onshore Frio petroleum province and have similarities that link them with fields in the lesser explored offshore Frio. Production trends offshore were also traced using all offshore Frio fields with cumulative productions greater than 1 million

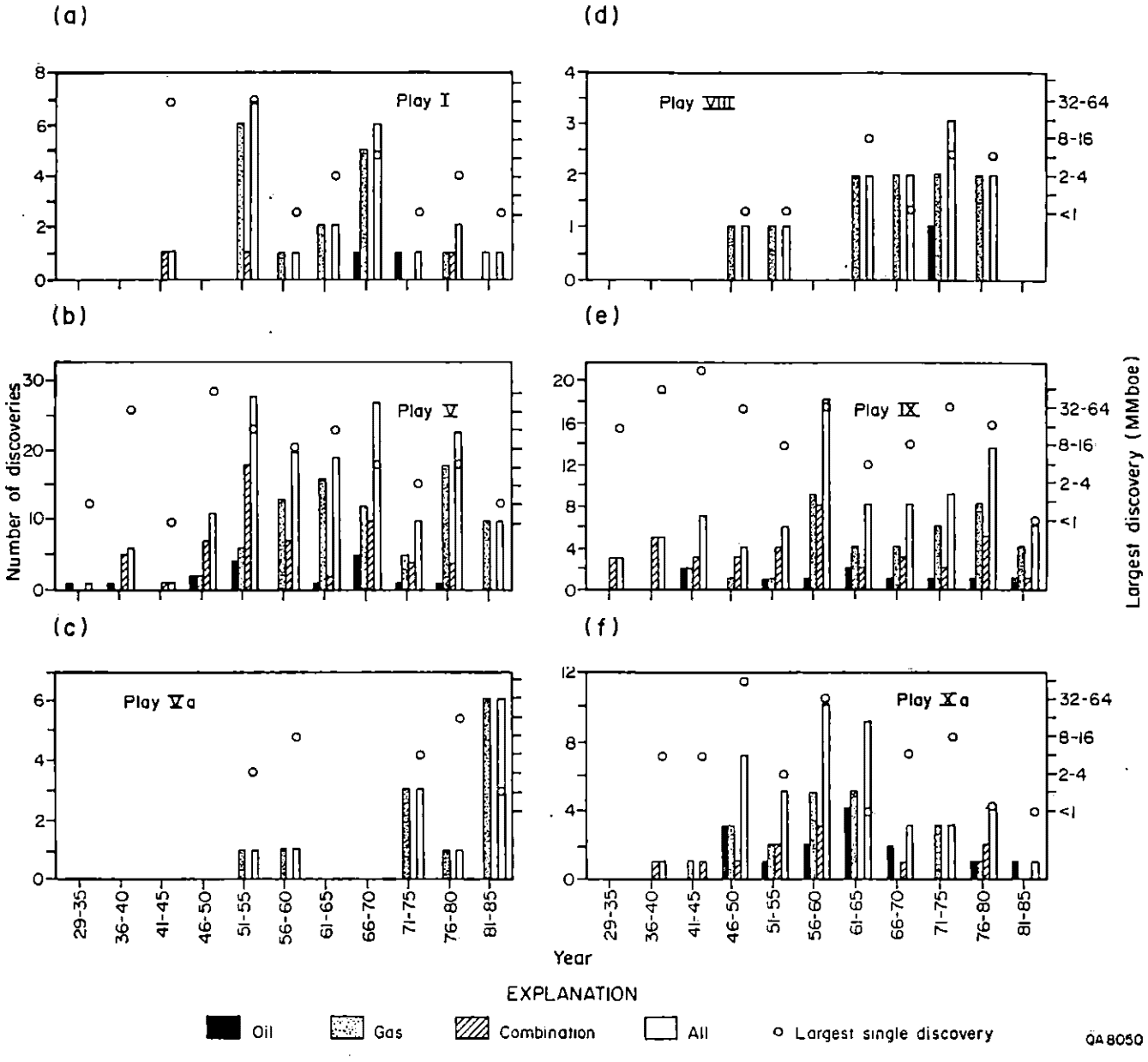

Figure 5. Plots of distal Frio new-field discovery history by play.

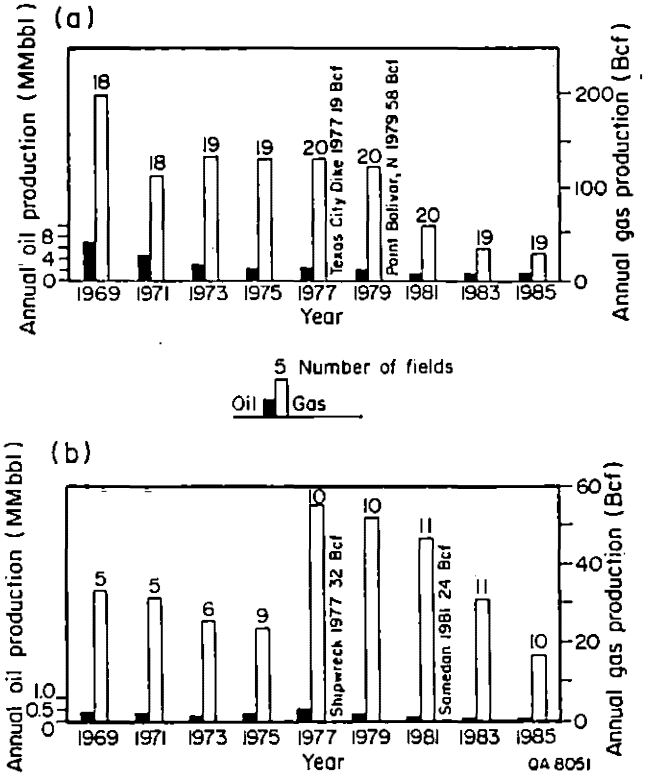

Figure 6. Distal Frio historical production trends. (a) All onshore fields with >10 million boe located in bays and lagoons. (b) All offshore fields with >1 million boe.

boe (fig. 6b). These 11 fields are listed in table 2. Production histories of individual fields are discussed in the section describing typical distal Frio fields.

Comparison of graphs of onshore and offshore production histories reveals information about the nature of exploration and production activity along the downdip margin of the prolific Frio trend. In general, fields in both groups are gas prone. Onshore fields have yielded much more oil and gas than have offshore fields because the onshore has been explored longer, drilling density is greater onshore, and the onshore Frio is shallower and richer in sandstone. Frequency of discovery, however, is relatively lower onshore than it is offshore (fig. 6). Gas production onshore dropped sharply in the early 1970's but then stabilized throughout the rest of that decade (partly owing to the contribution of two significant play IX gas discoveries, Texas City Dike and Point Bolivar North) before dropping again in the 1980's. Onshore oil production declined throughout this period. Offshore oil and gas production declined throughout the first half of the 1970's (fig. 6b), even though four new discoveries were made (table 2). Discovery of the Shipwreck (play IX) and Samedan (play Va) gas fields boosted total offshore production to its peak between 1977 and 1981. In the last several years, however, offshore production has dropped again, and no big discoveries have been made since Samedan. In general, onshore production probably peaked during the 1960's, and whereas the offshore seems to be about 10 years behind, more discoveries like Shipwreck and Samedan could reverse that trend. Federal pricing regulations and market conditions may influence the production trends shown in figure 6.

Table 2. Discovery history of offshore Frio fields having cumulative productions greater than 1 million boe.

Discovery Year	Field/Offshore Area	Play	Total Production (10^6 boe)
1954	Chevron/Mstg. Isl.	V	28.0
1955	Mstg. Isl. Block 889	Va	3.0
1957	GOM-ST-904/Mstg. Isl.	Va	15.9
1961	Dunn-McCampbell/Mstg. Isl.	V	6.6
1968	Sprint South/Mstg. Isl.	I	6.4
1972	Padre North/Mstg. Isl.	V	3.1
1973	Mstg. Isl. Block 883	Va	6.7
1974	Mstg. Isl. Block 749	Va	4.5
1975	Caplen South/Galv.	IX	1.1
1976	Shipwreck/Galv.	IX	25.0
1979	Samedan/Mstg. Isl.	Va	19.0

REGIONAL RESERVOIR CONDITIONS

Reservoir quality and temperature/pressure conditions in the distal Frio have been delineated regionally by using well log data and extrapolating from detailed investigations of the proximal Frio onshore. Suggested trends aid in ranking the exploration potential of broad areas but should not be used to predict site-specific favorability.

Porosity Trends from Acoustic Logs

Interval transit time (ITT) from acoustic (sonic) logs is the reciprocal of velocity of the compressional sound wave through rock and can be used to characterize sediment consolidation and compaction history. Loucks and others (1984, 1986) used abundant whole-core and acoustic log data to analyze regional trends of consolidation/compaction and porosity/permeability of lower Tertiary sandstones along the Texas Gulf Coast. They found that sandstone porosities are directly proportional to sandstone ITTs (fig. 7). Shale ITTs are proportional to the degree of dewatering and compaction (or undercompaction, as is the case in geopressured sediments [fig. 8]).

Loucks and others (1984, 1986) also found that reservoir quality in onshore Frio sandstones increases up the coast from South Texas toward Louisiana. Similarly, permeability, porosity, and sandstone ITT all increase from the lower to the upper Texas Gulf Coast--phenomena, they concluded, for which sandstone compositions and diagenetic processes are responsible. Frio sandstones along the upper Texas coast are rich in quartz and feldspar, whereas volcanic rock fragments are abundant in Frio sandstones in South Texas. These unstable rock fragments tend to enhance cementation and deform ductily, blocking pore throats.

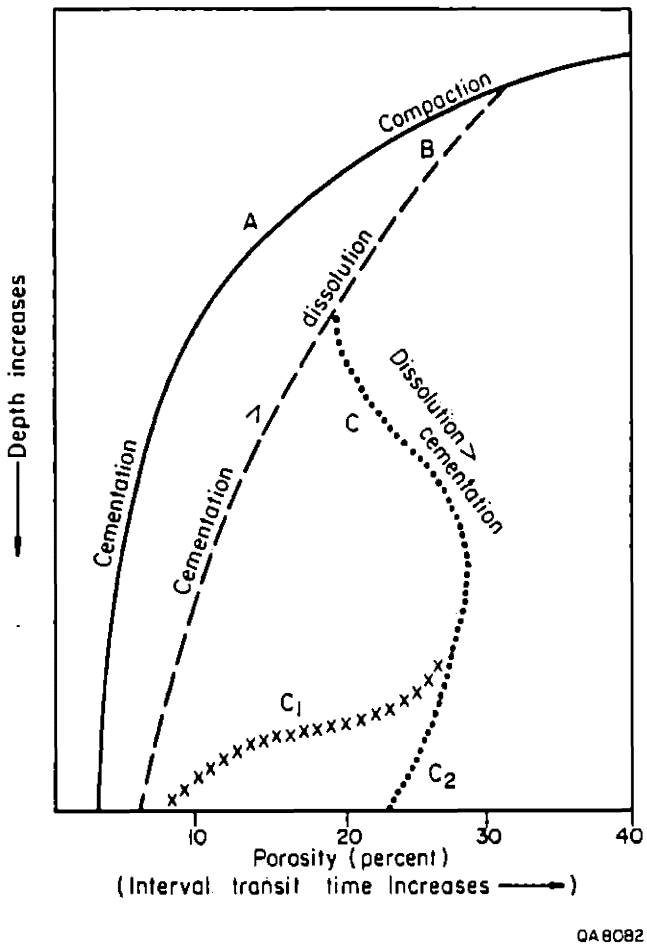

Figure 7. General trends of sandstone porosity and ITT with depth. Curve A shows loss of primary porosity with depth by compaction and cementation; no secondary porosity developed. Curve B represents porosity loss with depth where compaction and cementation rates are greater than the rate of secondary porosity production. Curve C shows porosity loss with depth by compaction and cementation followed by a major zone of porosity enhancement caused by secondary dissolution. Curve C_1 indicates a late stage of porosity-destroying cementation, whereas curve C_2 indicates porosity preservation with further burial. From Loucks and others (1986, their fig. 25).

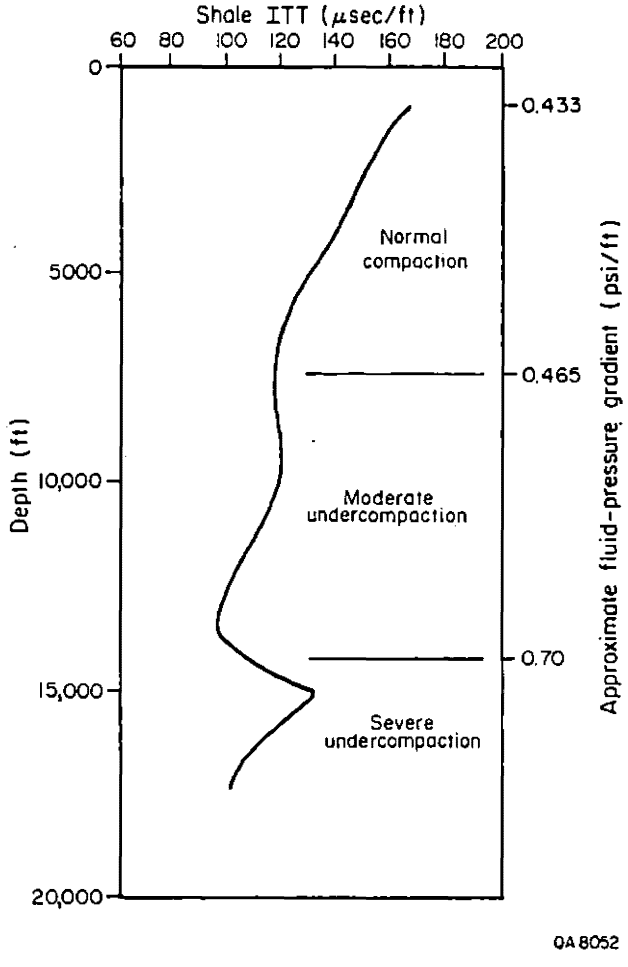

Figure 8. Generalized trend of shale ITT versus depth, Frio Formation. Moderate undercompaction begins where fluid-pressure gradients exceed hydrostatic (0.465 psi/ft). Severe undercompaction occurs where fluid-pressure gradients exceed 0.70 psi/ft. The zone of moderate undercompaction is generally considered transitional between hydropressured and true geopressured conditions (severe undercompaction). Modified from Galloway and others (1982, their fig. 29).

Using available acoustic logs from deep wells along the coast and offshore (fig. 9), we delineated general porosity trends in the distal Frio. Shale compaction and geopressure were also analyzed. Sandstone and shale ITT-versus-depth plots were compared for the three major depositional subdivisions of the distal Frio: the Norias delta system in South Texas (fig. 10), the Greta/Carancahua barrier/strandplain system along the middle Texas coast (fig. 11), and the Houston delta system along the upper Texas coast (fig. 12). Comparisons were also made between shallower hydropressured areas and deeper geopressured areas.

Compaction trends in distal Frio shales are relatively consistent along the entire Texas Gulf Coast. In more proximal wells, shale ITTs decrease steadily with depth (figs. 10a and 12a). The Frio in these areas is hydropressured to transitionally geopressured (compare with figure 8). Figures 10b and 11a show an increase in shale ITTs near total well depth, indicating the top of the zone of severe undercompaction (generally picked as the operational top of geopressure [fig. 8]). In more distal wells, shale ITTs increase sharply in Anahuac shales above the Frio (figs. 10c, 11b and c, and 12b and c), indicating that the entire underlying Frio interval is geopressured.

Porosities in deeply buried (>8,000 ft [2,440 m]), clean (clay-free), consolidated sandstones can be derived from ITTs using the time-average relationship (Gardner and others, 1974; Gregory, 1977). Basic sandstone ITT/porosity data for each of the major distal Frio depositional systems are shown in figure 13. Although porosities generally decrease with depth, large variations exist. Geopressured sandstones generally have higher porosities than do hydropressured sandstones at similar depths (fig. 13). This is attributable to two factors: formation of secondary porosity and decrease of effective (lithostatic) pressure on the sand framework owing to an increase in pore-fluid pressure. In

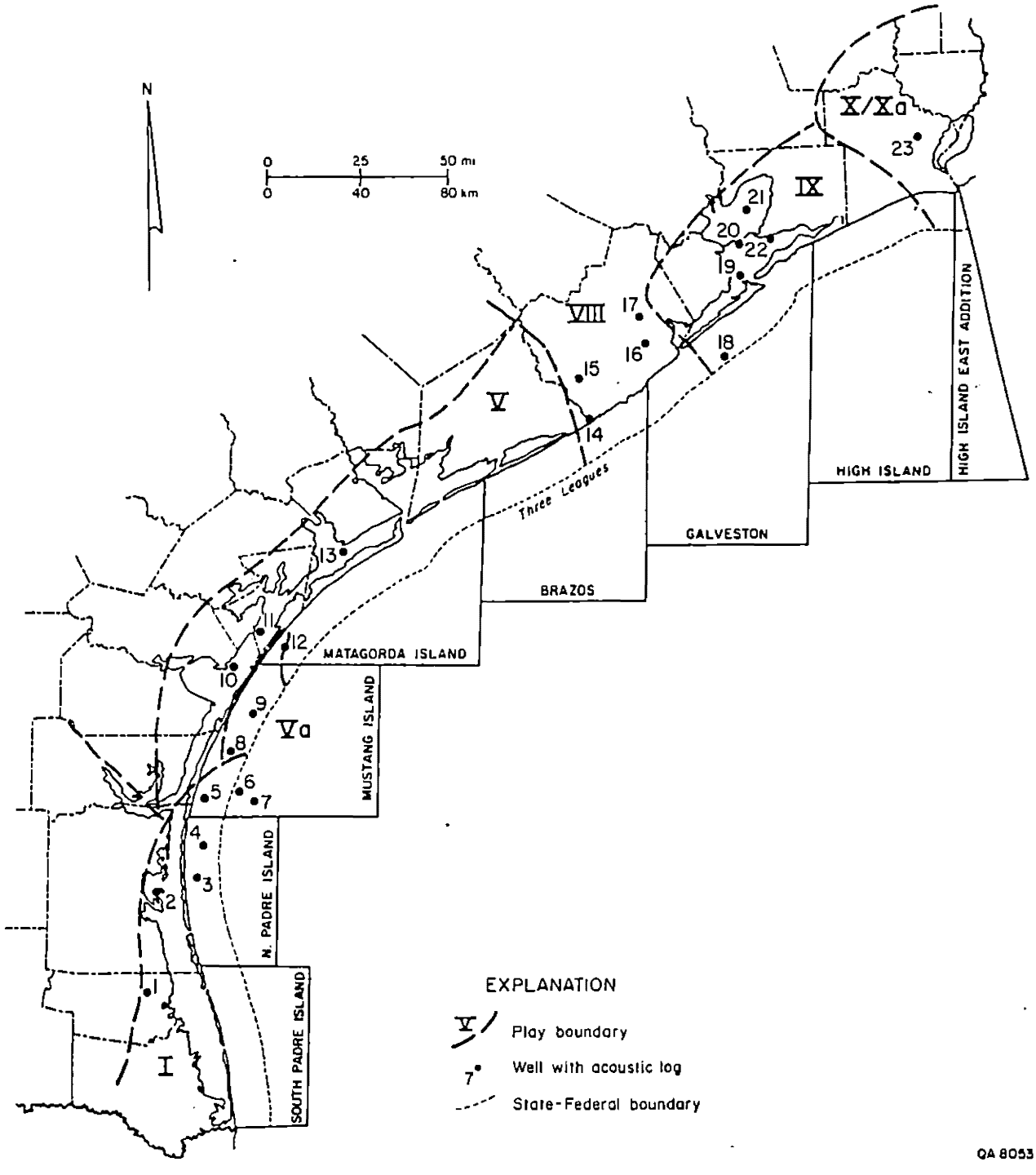

Figure 9. Location of acoustic well log control, distal Frio Formation. Wells identified in appendix D.

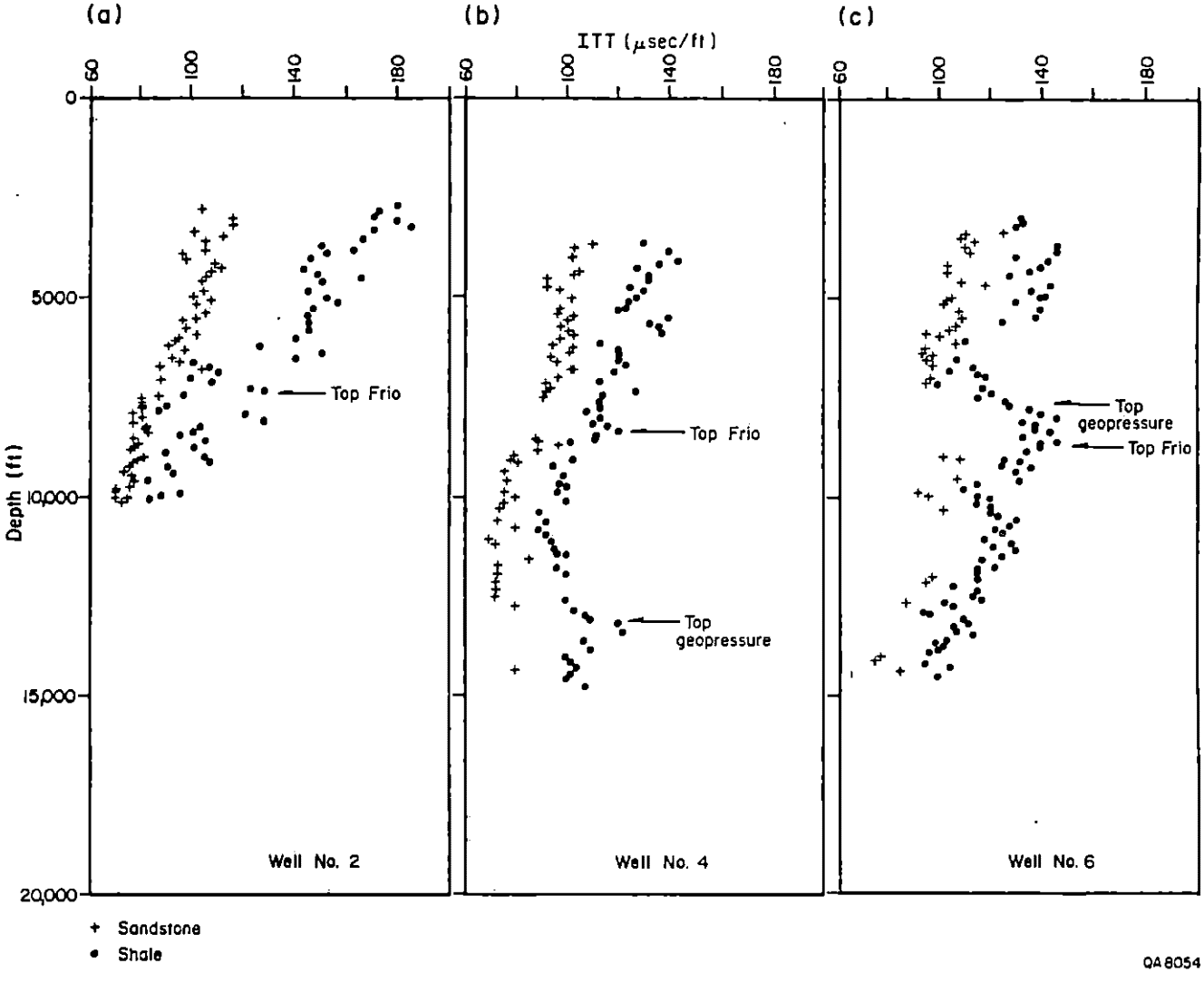

Figure 10. Typical plots of ITT versus depth for the Norias delta system (play I). Well locations shown in figure 9.

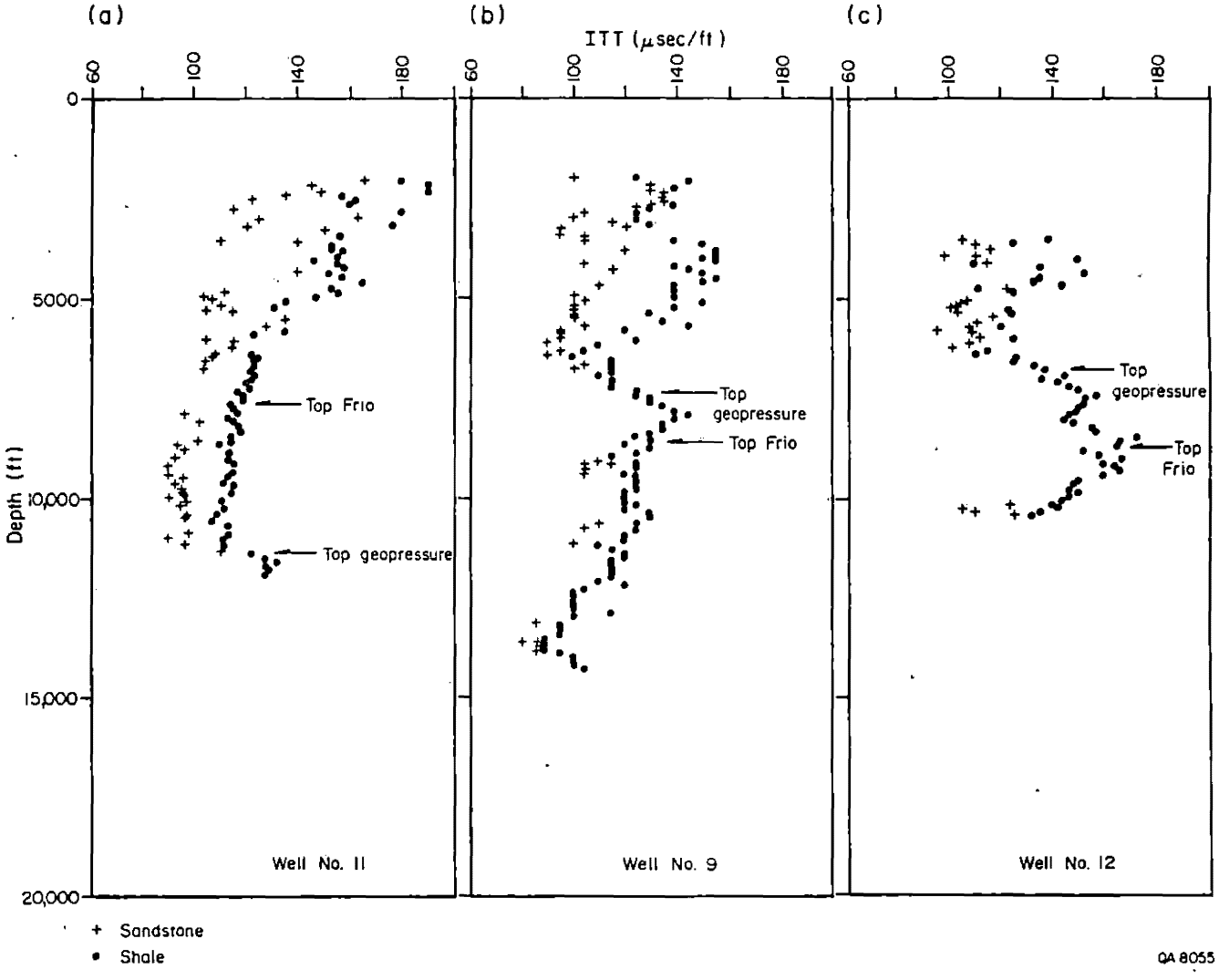

Figure 11. Typical plots of ITT versus depth for the Greta/Carancahua barrier/strandplain system (plays V and Va). Well locations shown in figure 9.

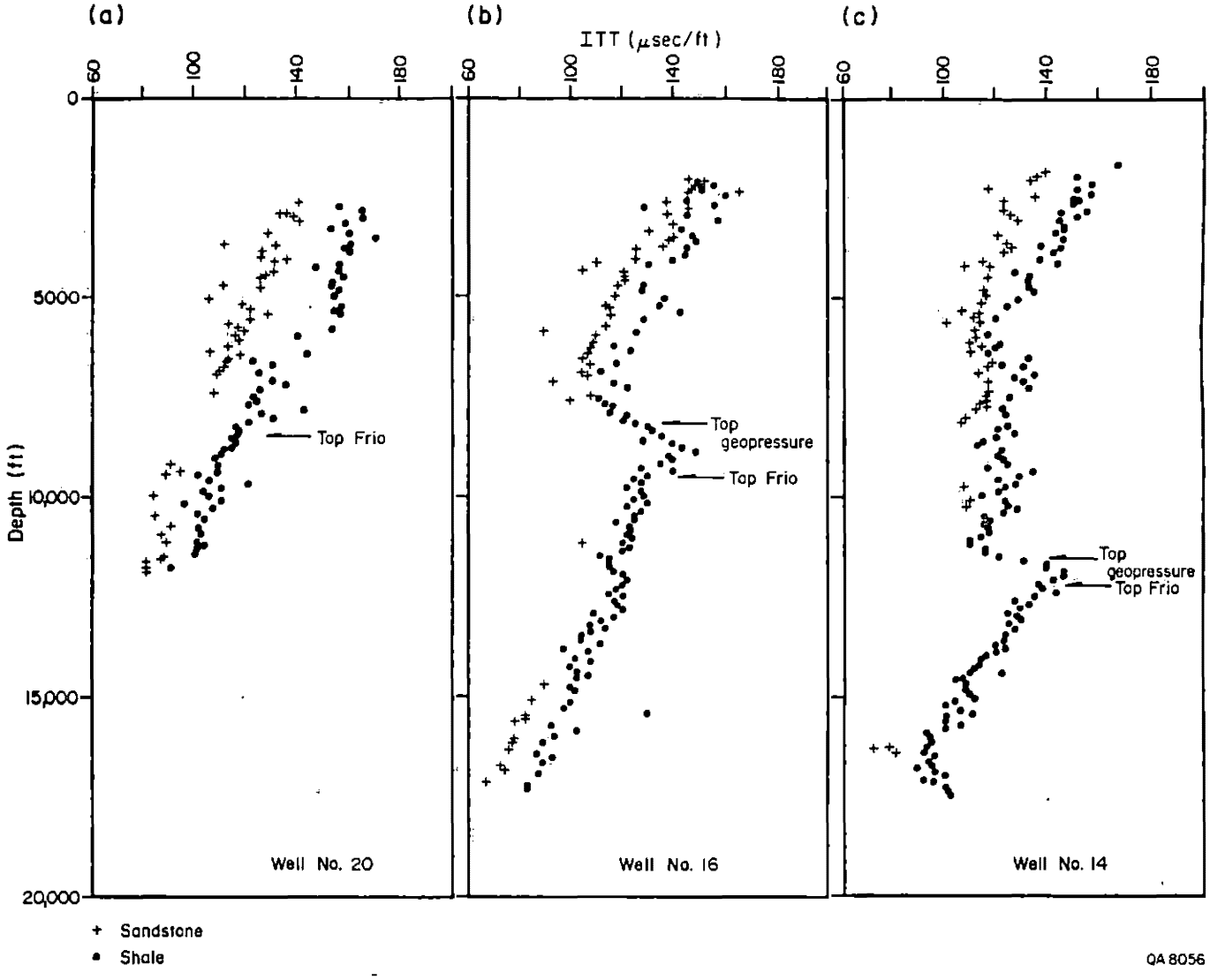

Figure 12. Typical plots of ITT versus depth for the Houston delta system (plays VIII and IX). Well locations shown in figure 9.

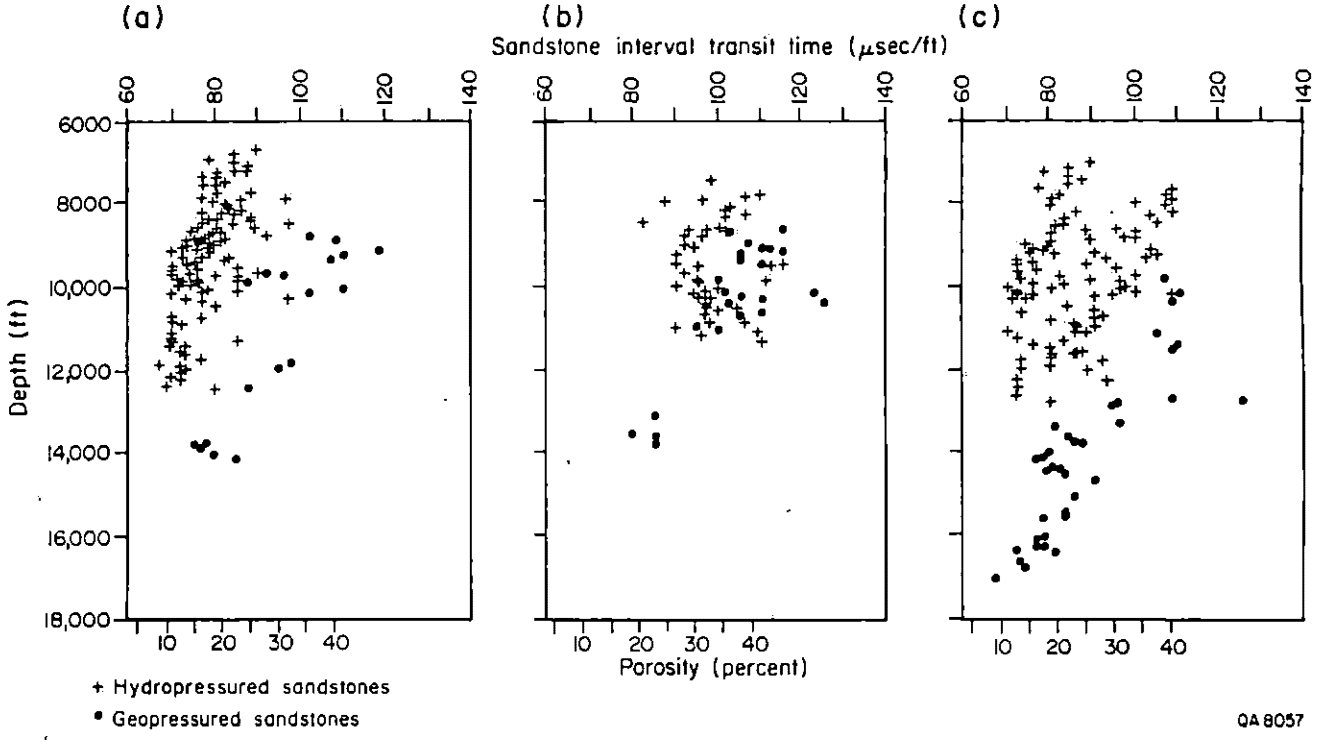

Figure 13. Basic data for trends of sandstone ITT versus depth, Norias and Houston delta systems and Greta/Carancahua barrier/strandplain system. Porosity scale is based on the time-average relationship (Gardner and others, 1974), which is most accurate for consolidated sandstones that are relatively free of clay matrix and saturated with saline fluid. ITT measurements were taken only in sandstones considered, on the basis of interpretation of spontaneous potential (SP) and resistivity log patterns, to have met these conditions. Apparent porosities greater than 40 percent, however, are likely overestimations attributable to the presence of clay matrix, gas, or both.

well-consolidated sandstones at depth, the effect of secondary porosity formation should be greater than that of reduced effective pressure (Gardner and others, 1974). Secondary porosity is formed by dissolution of both framework grains (especially feldspars) and cements.

Regional sandstone porosity trends of the three major distal Frio depositional systems were compared by visually fitting curves to the basic data shown in figure 13 and combining those curves on a single graph (fig. 14). These curves delineate complex patterns of porosity variation with depth, thereby displaying the relative effects of cementation and dissolution (compare with figure 7). Cementation reduces porosity with depth in hydropressured sandstones between about 7,000 and 9,000 ft (2,134 and 2,744 m). Between 9,000 and 12,000 ft (2,744 and 3,659 m), zones of secondary porosity formation occur in hydropressured sandstones in the Houston delta and Greta/Carancahua barrier/strandplain systems (fig. 14). In hydropressured sandstones in the Norias delta system, the rate of porosity-destroying cementation decreases below 10,000 ft (3,049 m), but no zone of enhanced porosity is present.

In all three systems, well-developed zones of secondary porosity are present in the shallower parts of the geopressured zone (fig. 14), although, as mentioned previously, relatively higher apparent sandstone porosities in the geopressured zone are due partly to a decrease in lithostatic pressure. Additionally, decrease in the lithostatic load (and concomitant increase in pore-fluid pressure) may enhance preservation of secondary porosity by inhibiting collapse of secondary pores. Reduced pore-fluid salinities are sometimes present near the top of the geopressured zone, an area characterized by complex rock-water interactions, variations in fluid flow, and thermal (or haline) convection (Morton and Land, 1987). In the proximal Frio, secondary porosity is also abundant near the top of geopressure (Loucks and others, 1984, 1986). Thus, there is a complex interplay

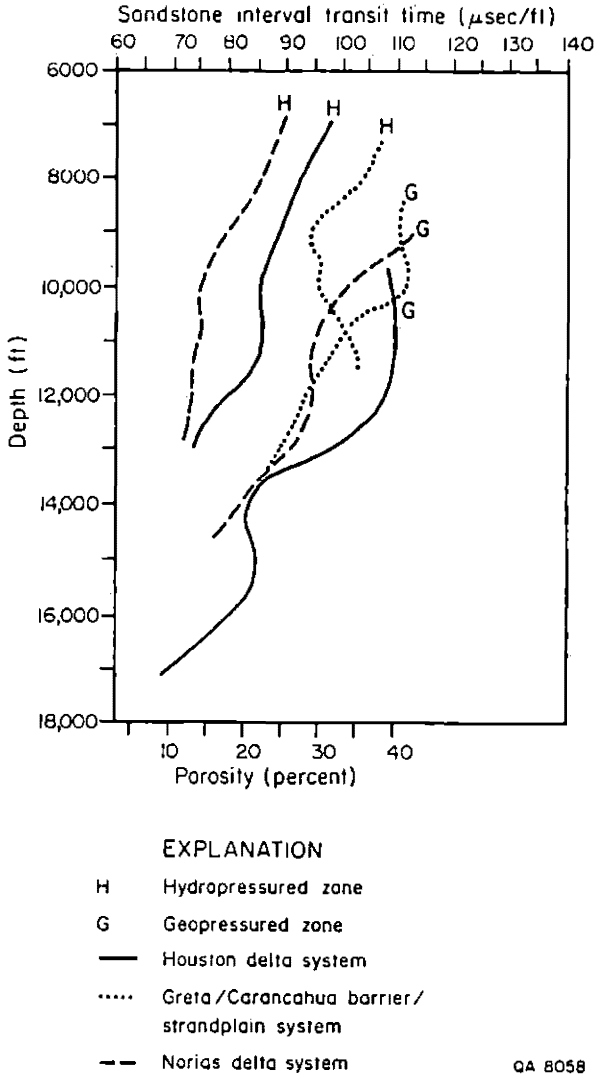

Figure 14. Trends of sandstone ITT/porosity versus depth for each major depositional system and for hydropressured and geopressured conditions. Curves are visual best-fit lines drawn through the data shown in figure 13.

of processes in the shallower parts of the geopressured zone and in the overlying transitional zone (0.465 to 0.70 psi/ft) that commonly has a net effect of enhancing porosity. However, much secondary porosity is destroyed in the deeper parts of the geopressured zone by late-stage cementation (fig. 13; compare with fig. 7, curve C_1).

Reservoir quality of deep-water, continental slope sandstones of the Frio Hackberry (play Xa) was also analyzed using the ITT-versus-depth approach. Figure 15 shows that deep Hackberry submarine channel-fill sandstones have porosities equal to or greater than those in barrier/strandplain sandstones of the upper Frio. Top of geopressure occurs below these upper Frio sandstones but above the Hackberry (fig. 15).

The same regional trend of increasing porosity from the lower to upper Texas coast that is characteristic of the proximal Frio (Loucks and others, 1984, 1986) also applies to the distal Frio with one major exception: the highest porosities above 10,000 ft (3,049 m) occur along the middle Texas coast in the Greta/Carancahua barrier/strandplain system (fig. 14). In deep geopressured sandstones between 10,000 and 13,000 ft (3,049 and 3,963 m), porosities are highest along the upper coast in the Houston delta system. Porosity trends in geopressured sandstones of all three systems converge at about 14,000 ft (4,268 m). A deep zone of secondary porosity occurs in lower Frio sandstones in the Houston delta system at about 15,000 ft (4,573 m) (fig. 14); acoustic log data were unavailable for the other two systems at this depth.

A trend of northward-increasing porosity occurs throughout the Norias delta system. Porosity differences between geopressured and hydropressured sandstones are most pronounced in this system (figs. 13a and 14). The reason is partly

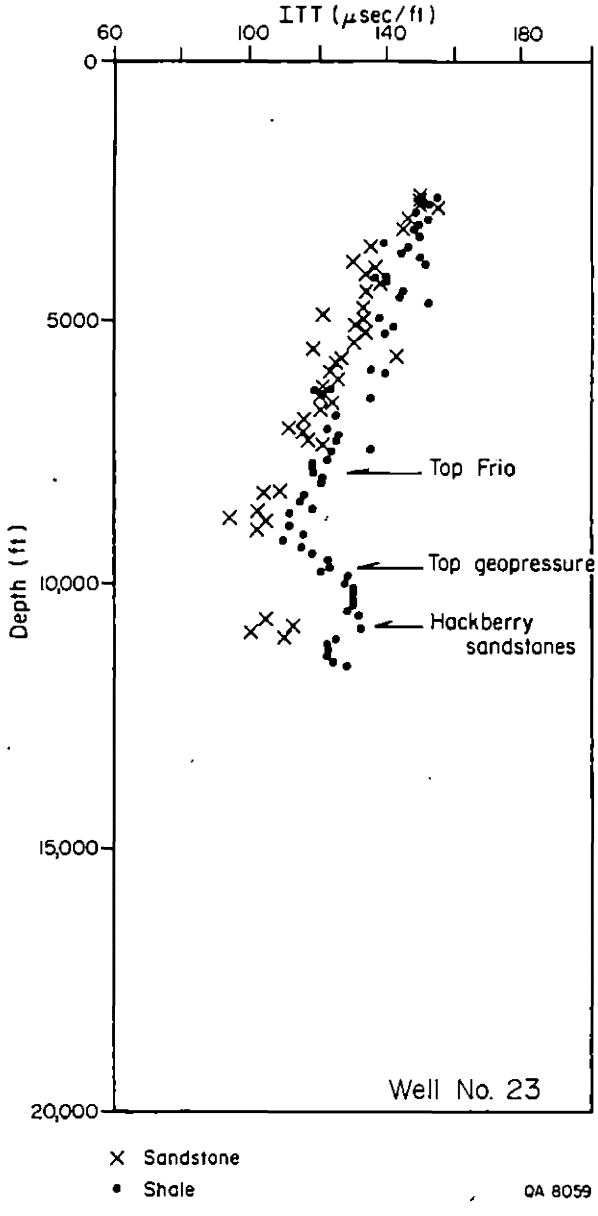

Figure 15. Plot of ITT versus depth for the Hackberry slope system (play Xa). Well location shown in figure 9.

geographical: hydropressured sandstone data are all from wells 1 through 4, located in the center of the delta, whereas geopressured data are from wells 5 through 7 on the northern margin of the delta (fig. 9).

According to this regional survey, distal Frio sandstone porosities are highest in the shallow parts of the geopressured zone in two areas: (1) the offshore Mustang Island Area around the northern fringe of the Norias delta system and the southern margin of the Greta/Carancahua barrier/strandplain system (play Va and adjacent parts of plays I and V [pl. 5]) and (2) in the Houston delta system along the upper Texas coast (plays VIII and IX [pl. 5]). This zone of enhanced porosity occurs between 8,000 and 10,000 ft (2,439 and 3,049 m) in the first area and between 10,000 and 13,000 ft (3,049 and 3,963 m) in the second area (fig. 14). Good reservoir quality in both areas is due mainly to the development and preservation of secondary porosity.

Temperature and Pressure Regimes

Fluid pressures in the deep distal Frio Formation are related to shale compaction, which in turn reflects the efficiency of fluid migration. Abundant thick sandstones generally have interconnected permeability conduits that allow adequate fluid circulation and pressure equilibration to near hydrostatic level. The low permeability of thick mudstone intervals that contain only isolated sandstones inhibits fluid migration and results in overpressuring (geopressure). Geopressure can therefore be related regionally to gross sandstone content.

Subsurface temperature and geothermal gradient are influenced by pressure and lithology. The geothermal gradient is higher through materials with lower thermal conductivity, such as clay and water, and lower through more conductive materials, such as quartz. The geothermal gradient should increase through fluid-

rich, undercompacted, high-shale intervals (Lewis and Rose, 1970). Restriction of fluid flow and thermal convection can also increase the geothermal gradient in geopressured sediments (Jones, 1975). In the Gulf Coast Tertiary System, the geothermal gradient typically increases through the geopressured zone (Gregory and others, 1980; Weise and others, 1981).

A contour map of temperatures at the top of the Frio Formation in the Coastal Zone (fig. 16) reflects the expected temperature increase with depth. Minimum distal Frio temperatures (those at the top of the interval) range from as low as 140°F (60°C), where top of the Frio is near 6,000 ft (1,830 m) deep, to greater than 280°F (138°C), where top of the Frio is greater than 12,000 ft (3,660 m) deep. Isothermal contour patterns along the upper Texas coast (fig. 16) can be correlated with the complex structural configuration caused by salt diapirism, lobate areas of higher and lower temperatures corresponding to withdrawal basins and domal uplifts, respectively (pl. 2a). At the southern tip of Texas and in adjacent offshore areas, high temperatures and straight strike-parallel isotherms reflect the great depths to the top and its steep descent across a series of large down-to-the-basin growth faults (pl. 2a).

Several strike-aligned areas of anomalously low temperatures extend from the northern part of the North Padre Island offshore area northeastward into the Matagorda Island offshore area (fig. 16). Elongate anticlinal shale ridges are common in this area, although only some of the larger ones are shown on the regional structure map (pl. 2a). These low-temperature zones may correspond locally to areas where the Frio is uplifted by shale diapirism. High sandstone content in the upper Frio along the shoreline adjacent to the North Padre Island and Mustang Island offshore areas (pl. 3a) may partly account for lower temperatures there. Vertical fluid flow through porous sand-rich zones reduces the geothermal gradient. Fault-related vertical permeability pathways can also permit upward thermal convection.

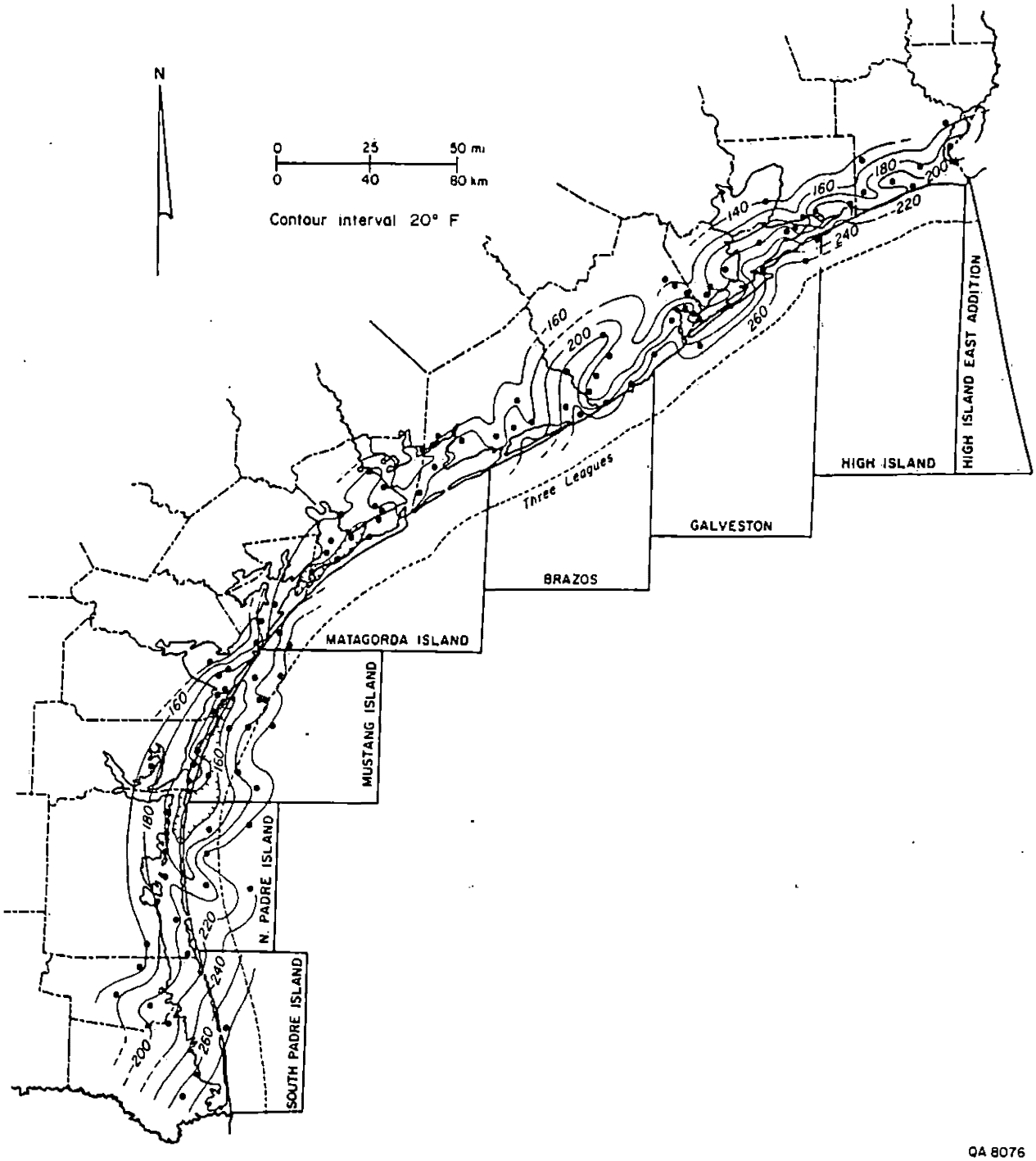

Figure 16. Contour map of temperature at top of the distal Frio Formation. Temperatures from well logs are corrected to approximate equilibrium according to the relation developed by Kehle (1971).

Figure 17 shows depths to the top of the Frio, the 200°F (93°C) isotherm, and geopressure along Galloway's (1986) regional strike cross section X-X''' (see plate 1 for location of section line), which approximately coincides with depositional strike. These features are also marked on distal Frio electric log dip sections (pl. 4). Along section X-X''', the Frio is 1,000 to 2,000 ft (305 to 610 m) deeper in the Houston delta system along the upper Texas coast than it is along the middle and lower coast (fig. 17).

In general, temperature does not exhibit a systematic trend or a well-defined relationship along section X-X'''. Depth to the 200°F isotherm varies between 8,000 and 9,000 ft (2,439 and 2,744 m) along most of the cross-section line (fig. 17) and does not seem to be influenced by large fluctuations in the top of geopressure, but may be responding somewhat to lithology. The isotherm rises above 8,000 ft (2,439 m) locally in the northeastern part of the Greta/Carancahua barrier/strandplain system and much of the Houston delta system (fig. 17), where thick shales (thermal insulators) in the upper Frio and overlying Anahuac Formations (pl. 4) may increase the geothermal gradient.

Top of geopressure can be regionally correlated with depositional systems and sand/shale ratios. The Norias delta system and adjacent parts of the Greta/Carancahua barrier/strandplain system are sand-rich, and top of geopressure is deep (fig. 17). Geopressure occurs at increasingly shallow depths northeastward through the barrier/strandplain system as this system becomes increasingly more mudstone dominated. Top of geopressure again descends in the Houston delta system (fig. 17), where sandstone content increases. Local fluctuations in depth to geopressure, 200°F, and the Frio in the Houston delta system are probably attributable partly to the complex structural setting of the Houston salt diapir province, where a dense network of growth faults is superimposed on diapiric uplifts, withdrawal basins, and related faulting. Throughout the Texas Coastal Zone in general, geothermal gradients and fluid-pressure conditions are highly

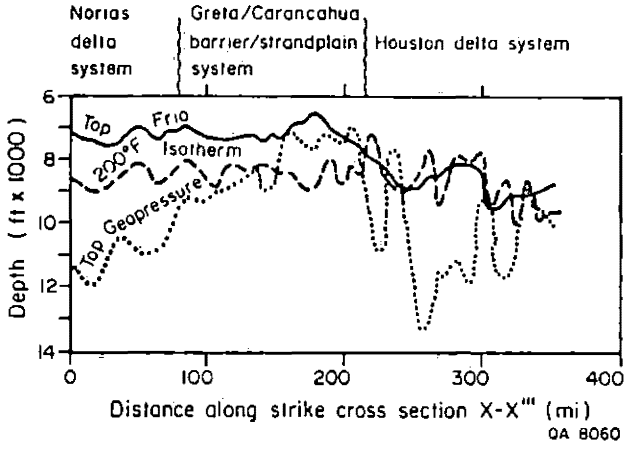

Figure 17. Depths to top of Frio, the 200°F (93°C) isotherm, and geopressure along regional distal Frio strike section X-X''' (see pl. 1 for line of section). Major distal Frio depositional systems shown at top. Geopressure occurs when fluid-pressure gradients equal or exceed 0.7 psi/ft.

variable, controlled locally by faulting, diapirism (salt and shale), lithology, permeability, and porosity.

Almost all of the distal Frio Formation offshore is hotter than 200°F (fig. 16) and therefore is within the temperature range of oil and thermal-gas generation (Galloway and others, 1982). Thick distal Frio mudstones could expel large volumes of hydrocarbons, which might then become trapped in interbedded sandstone reservoirs. The prime source rocks for onshore Frio oil and gas reserves are probably in the shallower parts of the undercompacted (geopressured) shale section (Galloway and others, 1982).

Historically, 90 percent of commercial oil in the Gulf Coast Basin has been found in the transitionally geopressured zone (0.465 to 0.70 psi/ft), whereas gas reservoirs with methane-saturated water drives are more abundant in deeper, severely geopressured (>0.70 psi/ft) sediments (Jones, 1975). Most new Frio discoveries offshore will probably be geopressured gas reservoirs.

DESCRIPTION OF TYPICAL FIELDS

Hydrocarbon fields in several distal Frio plays were selected for detailed description (fig. 18). Most of the fields described are either located offshore or thought to be typical of fields and potential new-field discoveries in offshore areas. Data availability was another constraining factor in the selection process. Fields in plays I, V, Va, and IX are described.

Play I, Norias Delta System

Although a large part of Frio play I extends offshore, discoveries in State waters have been made only along the northern margin of this play (fig. 19).

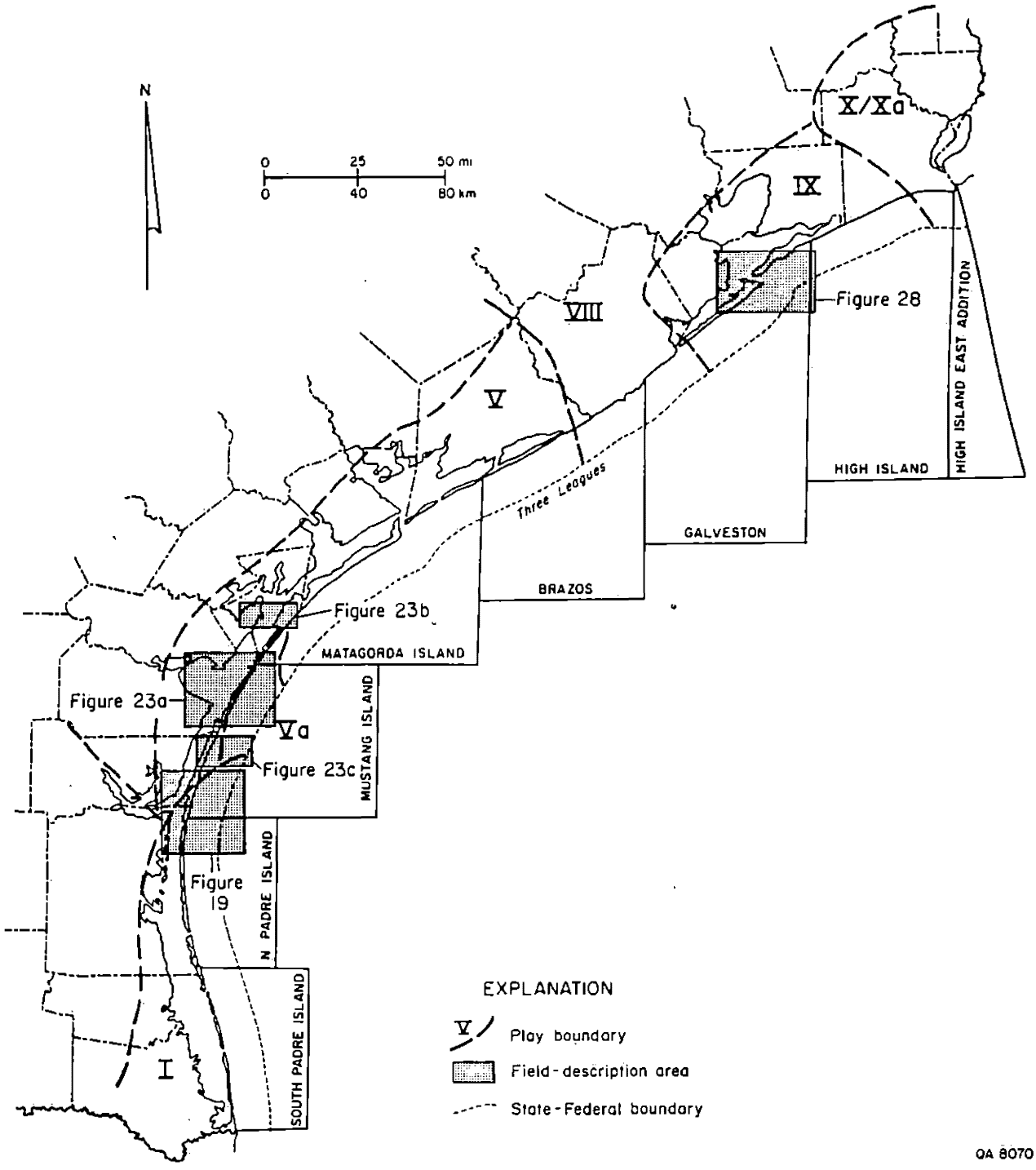

Figure 18. Locations of field-description areas shown in figures 19, 23, and 28.

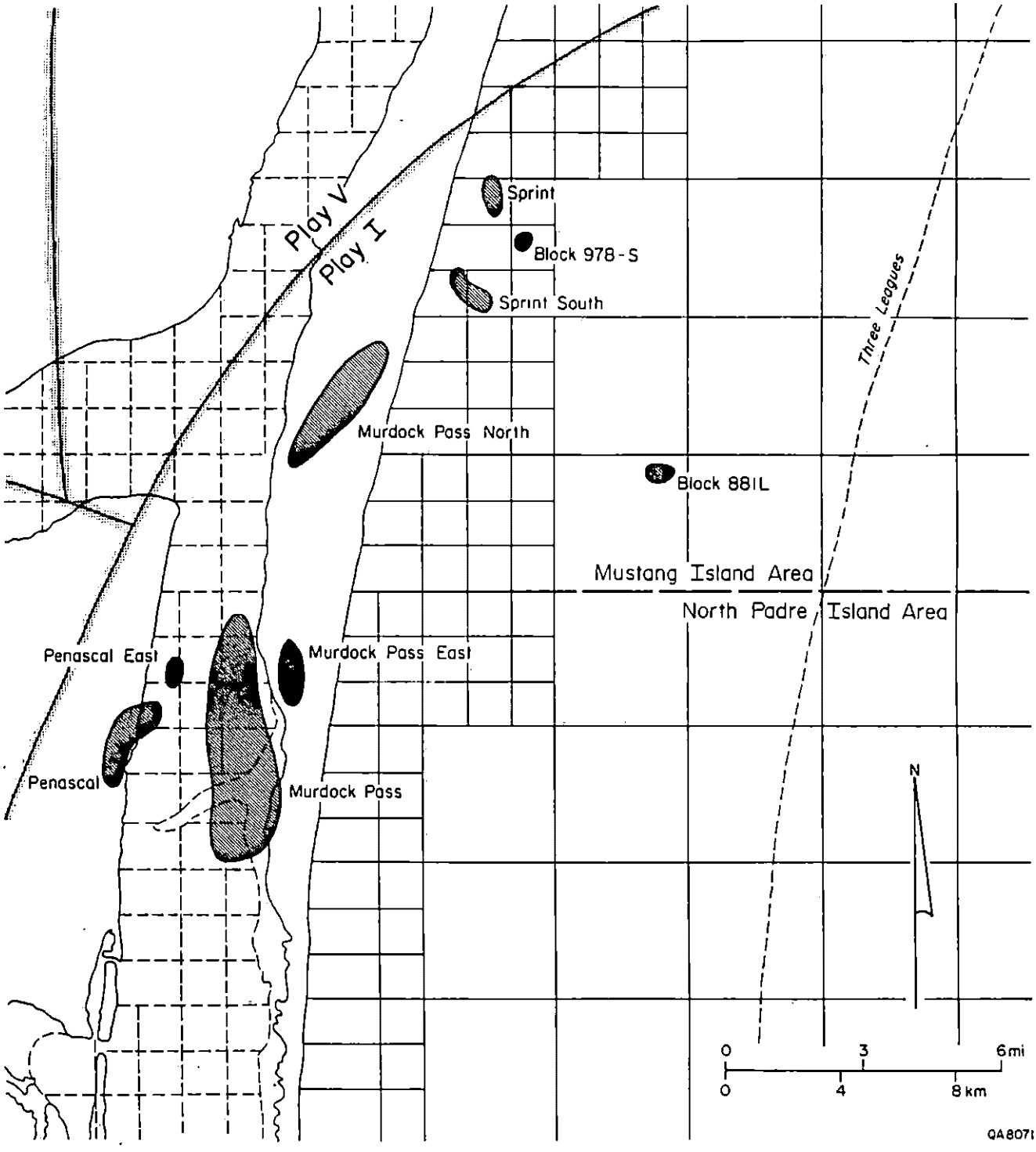

Figure 19. Locations of play I typical fields. See figure 18 for regional location of this map.

Sprint South (discovered in 1968) is the most prolific of the several small gas fields in play I in offshore State waters. The offshore fields, as well as the nearby Murdock Pass fields in Laguna Madre and on Padre Island, produce from middle and upper Frio sandstones in the Norias delta system. Reservoir sandstones generally cap sand-rich intervals below thick mudstones (fig. 20). In fact, most production is from Marginulina sandstones that underlie the transgressive Anahuac Shale. Sands, originally deposited in a delta-front environment, were winnowed and reworked at the onset of the succeeding marine transgression.

The structural setting for the offshore play I fields is relatively simple (fig. 21a and b). Sprint South gas is trapped in a rollover anticline on the downthrown side of a major growth fault. The productive area is further compartmentalized by an antithetic fault. The original Sprint field (discovered in 1954, now abandoned) produced from Frio zones deeper in this same fault block (figs. 20 and 21b). Gas production also occurs on the upthrown sides of both the major growth fault (Murdock Pass North, discovered in 1968) and the antithetic fault (Block 978-S, discovered in 1969) (fig. 21a and b).

Reservoir-quality data were unavailable for the offshore play I fields, but data from the Frio A reservoir (Marginulina sand, fig. 21c) in the Murdock Pass field (discovered in 1952) indicate that the reservoir properties of this uppermost Frio sand body are good. Average permeability and porosity of the Frio A zone are 200 millidarcys (md) and 24 percent, respectively, at Murdock Pass (Mulle, 1967).

Production trends during the last 15 years in the older but larger Murdock Pass field (total production 34 million boe) and the younger, smaller Sprint South field (6.5 million boe) are depicted in figure 22. Murdock Pass production declined sharply during the later 1970's and the 1980's, whereas Sprint South

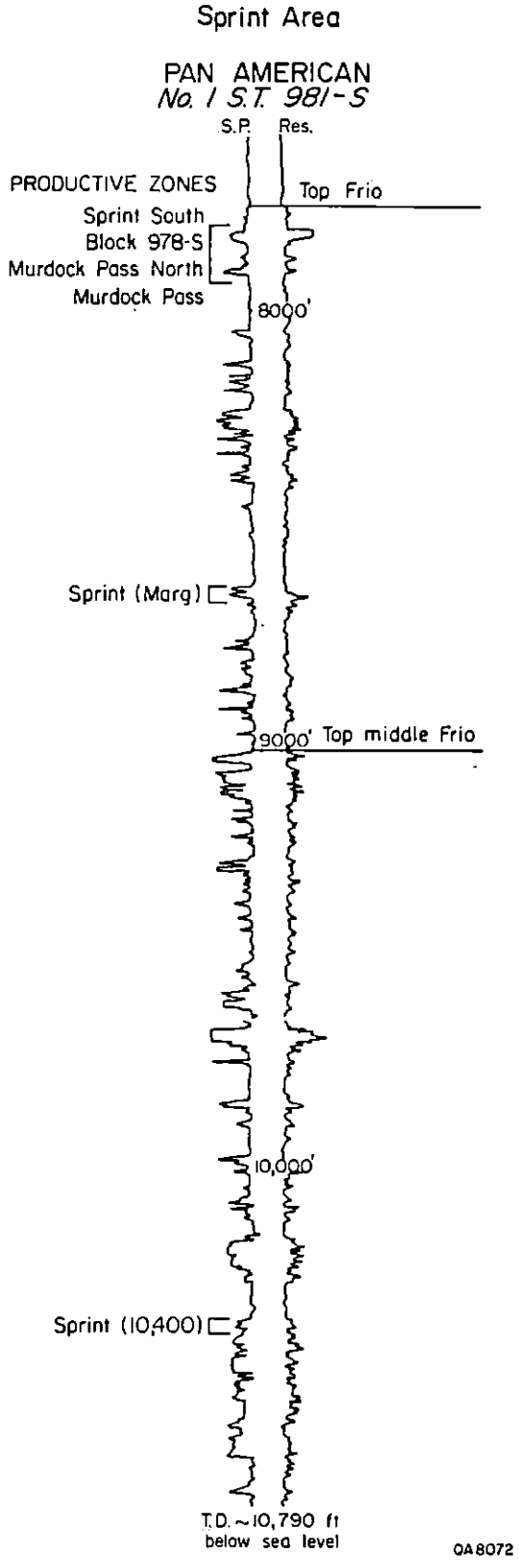

Figure 20. Typical electric log for play I fields in Sprint area, showing local producing zones. See figure 21a for well location.

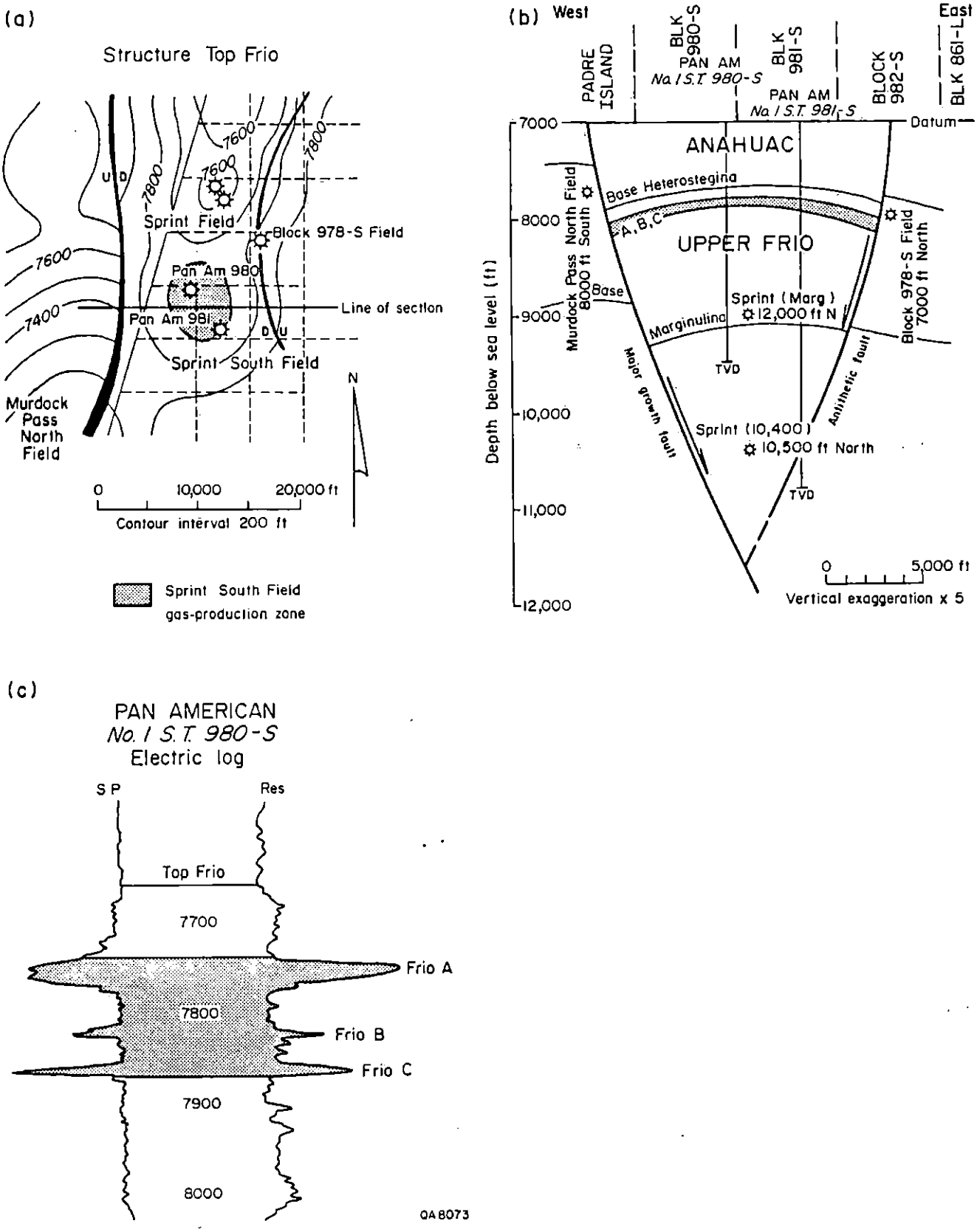

Figure 21. Sprint area (a) structure map, (b) structural cross section, and (c) electric log through Sprint South productive zone.

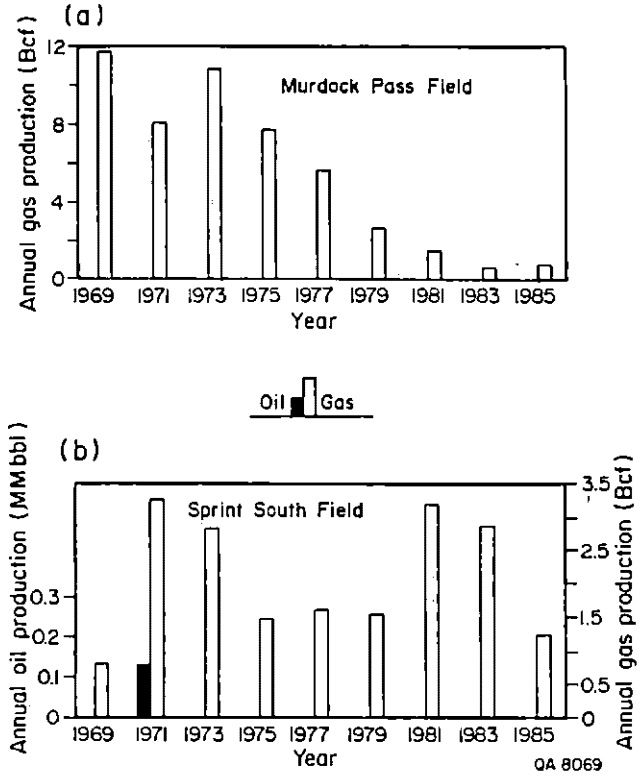

Figure 22. Historical Frio production trends, examples from play I.

production declined somewhat in the later 1970's but rose during the early 1980's. Since 1980, annual production at Sprint South has exceeded that at Murdock Pass.

Plays V and Va, Greta/Carancahua Barrier/Strandplain System

Frio play V and Va fields produce from barrier-bar, shoreface, and inner-shelf sand bodies in the Greta/Carancahua barrier/strandplain system. Frio fields are especially abundant and prolific in the southwestern part of this depositional system, close to the Norias delta system (pls. 5 and 6). Several fields in Corpus Christi Bay and adjacent offshore areas typify fields in plays V and Va (fig. 23a). Additional V and Va fields in Aransas Bay to the northeast (fig. 23b) and offshore from Kleberg County to the south (fig. 23c) are also described. The cross section in figure 24 shows typical logs, productive zones, and structural settings for the Corpus Christi Bay fields.

More updip play V fields, such as Encinal Channel (discovered in 1965), produce largely from thick, stacked barrier-core sandstones. Barrier-core facies grade downdip into thinner shoreface sandstones that are a combination of the distal margins of barrier complexes and storm-deposited inner-shelf facies (Galloway, 1986). Mustang Island (discovered in 1949), Mustang Island West (discovered in 1966), and several offshore gas fields (for example, GOM-ST-904, discovered in 1957; fig. 24) produce from these shoreface/shelf facies. To the northwest in Aransas Bay, Nine Mile Point gas field (discovered in 1965; fig. 23b) produces from very thin, fine-grained inner-shelf sandstones (fig. 25). In general, the more updip fields include numerous gas/condensate and oil reservoirs, whereas more downdip fields have fewer reservoirs and little liquid hydrocarbon production.

Offshore play Va fields include distal barrier shoreface/shelf facies but are also characterized by thicker sand bodies apparently transported along strike from

Figure 23. Locations of plays V and Va typical fields. (a) Corpus Christi Bay and adjacent offshore. (b) Aransas Bay. (c) Offshore Padre Island, Kleberg County. See figure 18 for regional locations of these maps.

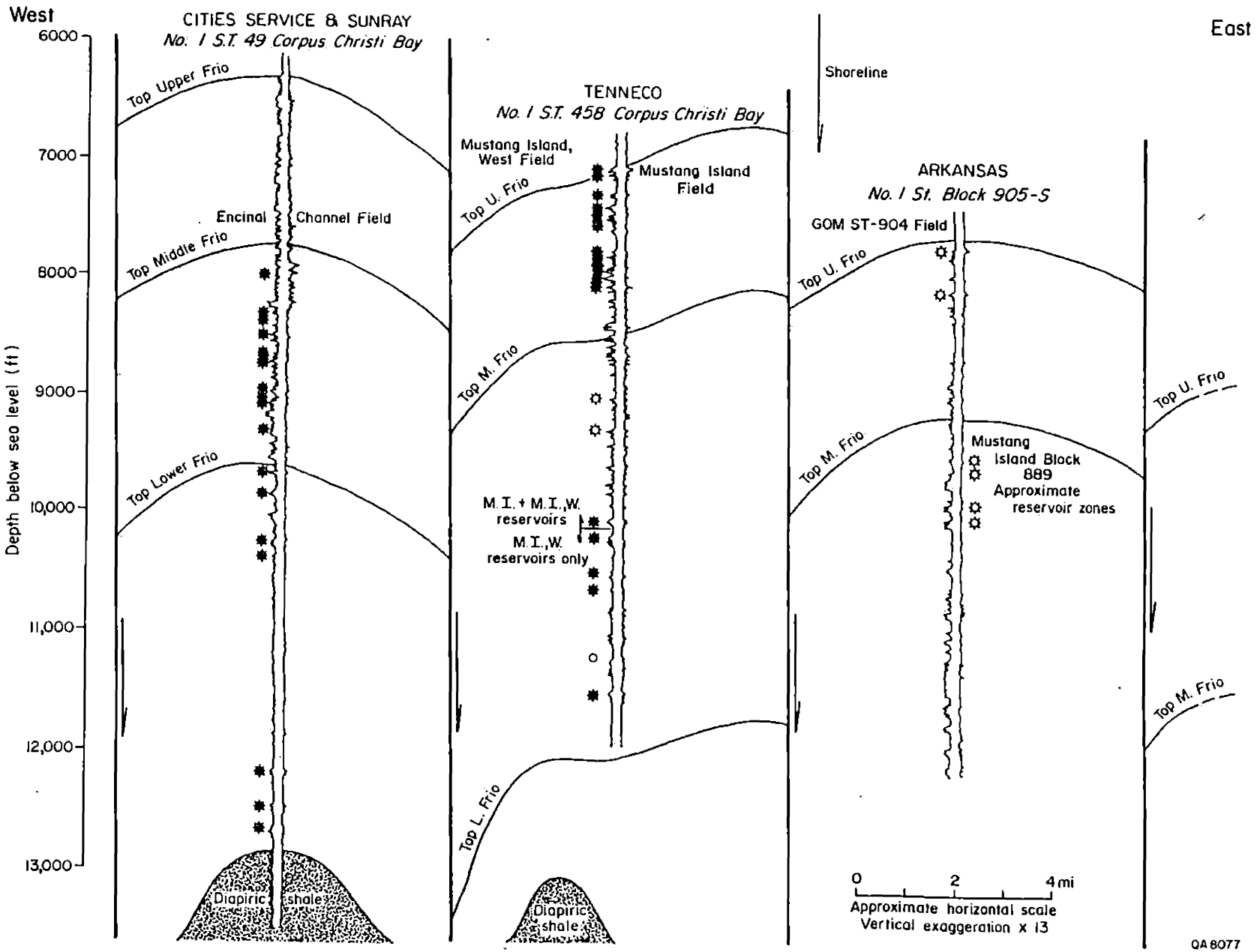

Figure 24. Structural cross section through Corpus Christi Bay and adjacent offshore area showing typical electric logs, producing zones, and structural styles in plays V and Va. See figure 23a for location of section line.

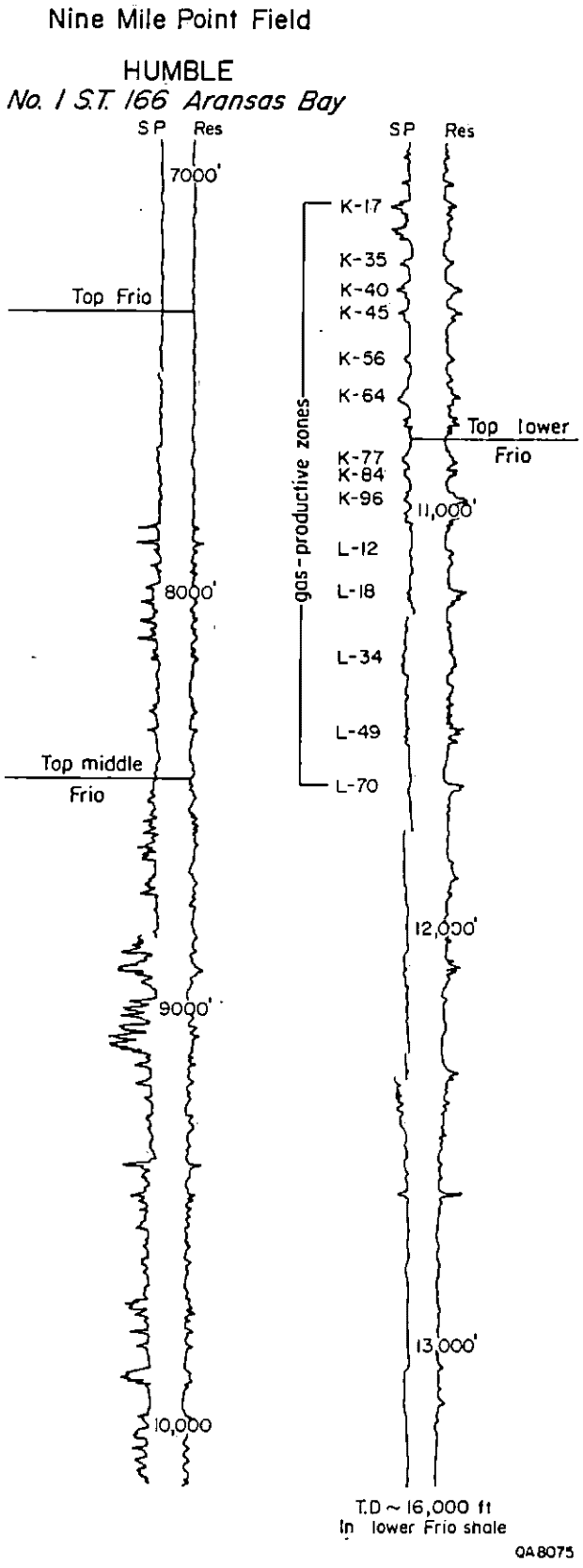

Figure 25. Electric log for Nine Mile Point field showing gas-producing zones. See figure 23b for well location.

the adjacent Norias delta system (deeper middle Frio section, most easterly log; fig. 24). Mustang Island Block 889 (discovered in 1955; figs. 23a and 24) and the prolific Samedan (discovered in 1979; fig. 23c) fields include some productive zones that may belong to this strike-reworked delta-fringe facies.

Play V and Va hydrocarbons are trapped by several types of structures. Encinal Channel and Mustang Island West reservoirs are arched over deep-seated diapiric mudstone, producing domal and anticlinal closure (fig. 24). Oil and gas in Mustang Island reservoirs are trapped on the upthrown side of a large growth fault (fig. 24). In Chevron field (discovered in 1954; fig. 23c), Frio production is also from upthrown fault closure (Kling, 1972). Nine Mile Point reservoirs occur in a complexly faulted rollover anticline. The offshore fields generally occur in growth-fault rollover anticlines and upthrown fault blocks.

Reservoir properties of play V and Va sand bodies are variable, but limited data suggest that porosity and permeability decrease downdip and along strike toward the northeast. On the southern margin of play V, three reservoirs in Chevron field (fig. 23c) have a mean permeability of 724 md (ranging from 654 to 863 md) and porosities ranging from 31 to 33 percent (Reynolds and Reese, 1967). Data from six Mustang Island reservoirs (Hicks, 1952) show a mean permeability of 417 md (ranging from 268 to 674 md) and a mean porosity of 28 percent (ranging from 27 to 31 percent). The two gas reservoirs in GOM-ST-904 have permeabilities of 112 and 110 md and mean porosities of 25 and 26 percent (Kling, 1972). Nine Mile Point gas reservoirs have the poorest quality; mean permeability and porosity from three zones (K17, K45, and K84; fig. 25) are 6.5 md and 19.5 percent (Berg and Powell, 1976). Therefore, in the Greta/Carancahua barrier/strandplain system, reservoir permeability and porosity

increase toward the barrier core (area of maximum sand buildup) and apparently also southwestward toward the northern margin of the Norias delta system.

Production has generally declined during the last 15 years in the play V and Va fields discussed here. Relative declines have been greatest in Mustang Island, Chevron, and GOM-ST-904 fields (fig. 26), whereas production in the younger Encinal Channel and Nine Mile Point fields declined during the early 1970's but leveled off somewhat in the late 1970's and early 1980's to between 1.5 and 3 Bcf of gas/year (fig. 27a and b). Mustang Island field had a similar period of production stability during the 1960's, producing about 1 million bbl of oil annually (fig. 26a). Production trends in the Chevron and GOM-ST-904 fields have been similar, both peaking around 1970 (fig. 26b and c). GOM-ST-904 field was relatively short lived, its two thin reservoirs producing 8 to 12 Bcf of gas annually for five or six years before falling off sharply, whereas Chevron, having 10 upper Frio reservoirs, maintained similar annual productions for more than twice as long. Samedan field appears to be near its peak, producing more than 20 Bcf of gas annually during the 1980's, although it declined somewhat in 1985 (fig. 27c).

Play IX, Houston Delta System

During the 1970's, several gas-prone fields were discovered around Galveston that produce from deep, distal delta-front sand bodies of the middle Frio: Texas City Dike (discovered in 1975), Texas City Dike North (discovered in 1976), Half Moon Shoal (discovered in 1976), Point Bolivar North (discovered in 1971), and the offshore field, Shipwreck (discovered in 1976) (fig. 28). The two reservoir sand bodies (Frio A and B; fig. 29) are relatively continuous across all these fields. In the discovery well at Shipwreck field (fig. 29), porosity and

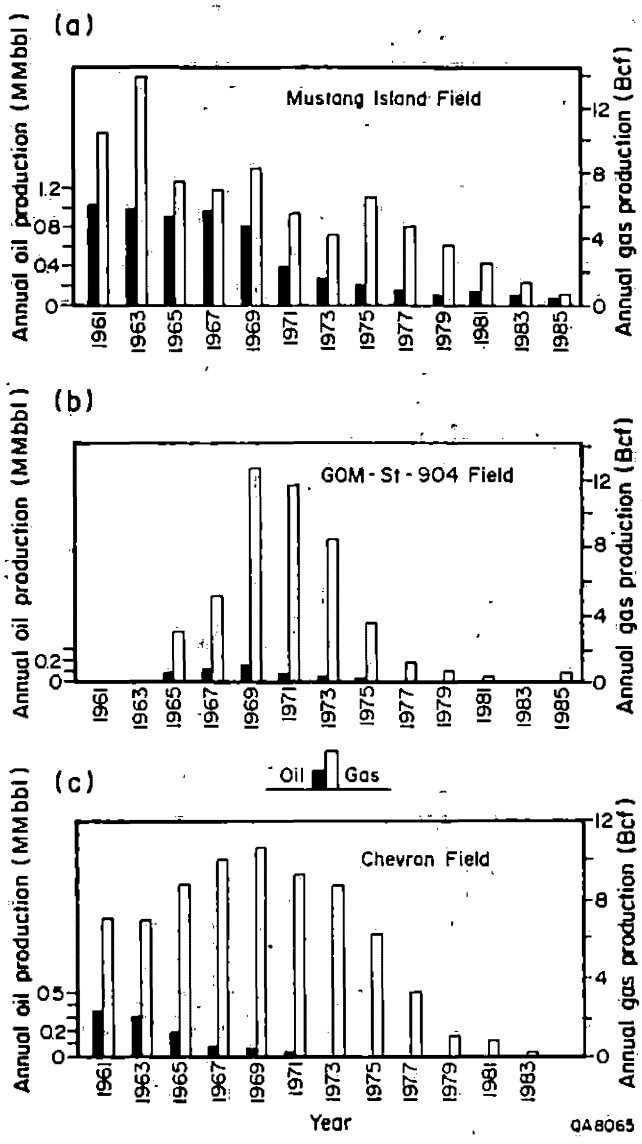

Figure 26. Historical Frio production trends, examples from older fields in plays V and Va.

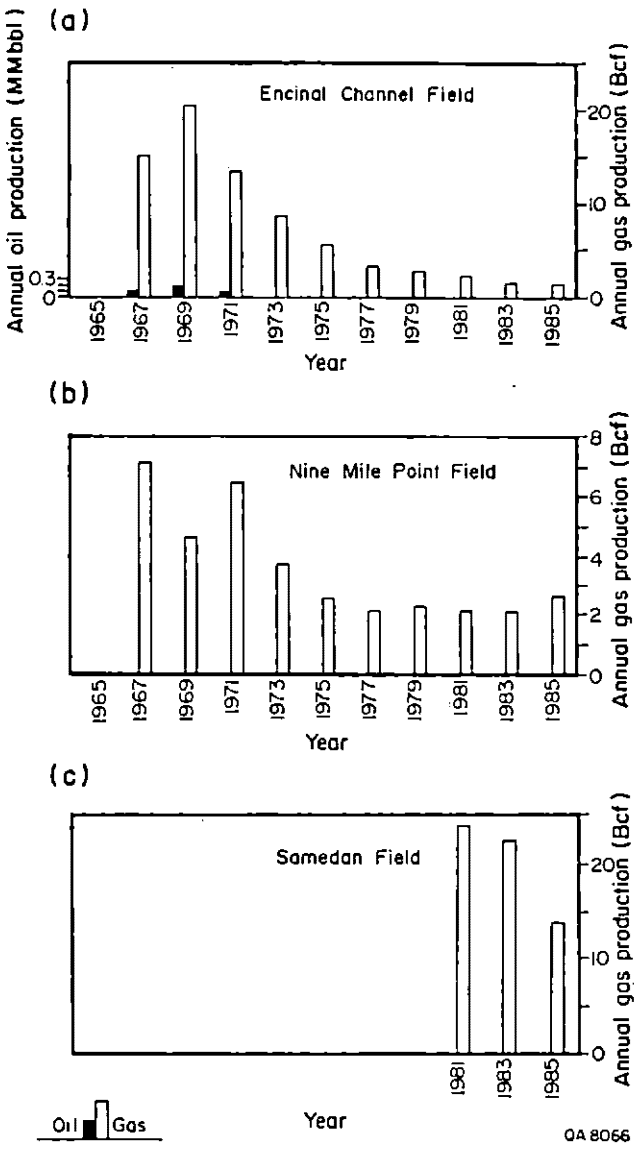

Figure 27. Historical Frio production trends, examples from younger fields in plays V and Va.

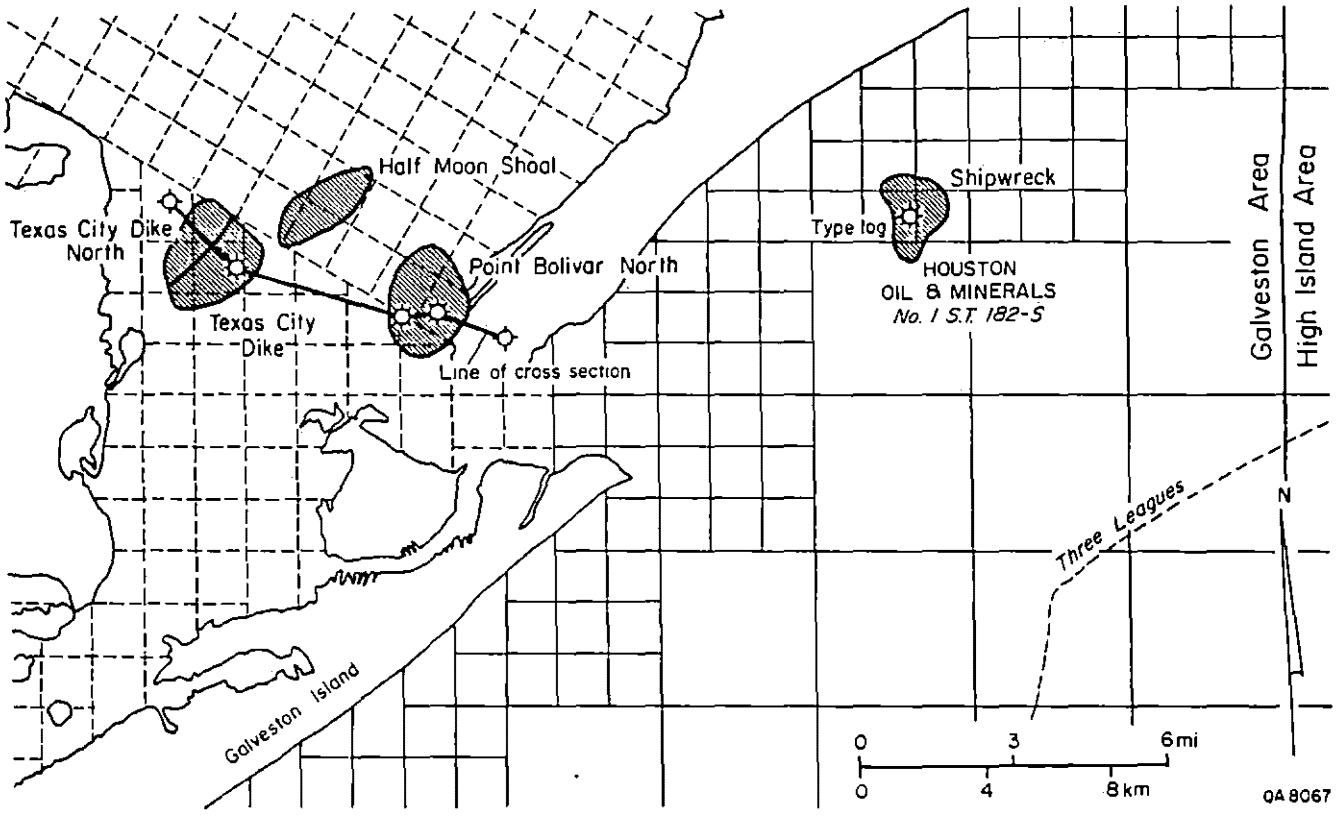

Figure 28. Locations of play IX typical fields. See figure 18 for regional location of this map.

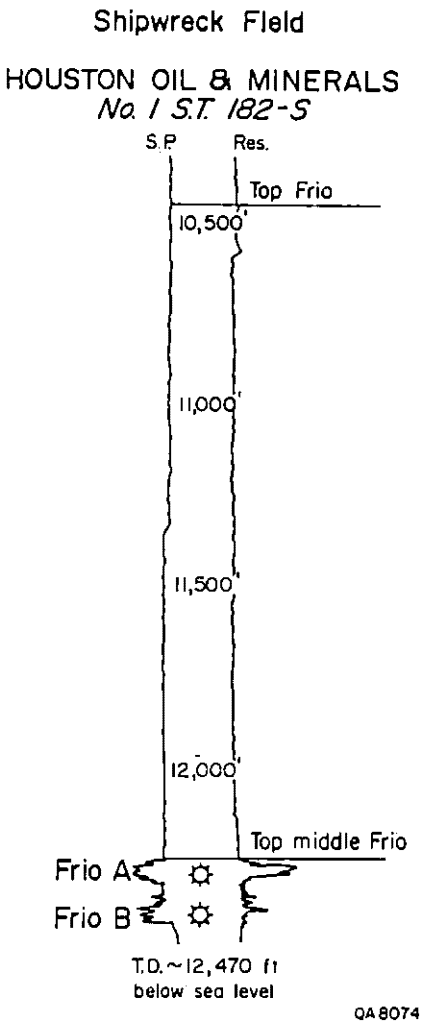

Figure 29. Electric log from the discovery well in Shipwreck field showing gas-productive Frio A and B sands. See figure 28 for well location.

permeability of the Frio B sand were measured at 29 percent and 107 md, respectively (Railroad Commission of Texas, Hearing Files). These delta-front sand facies may have been reworked during the marine incursion that transgressed the Houston delta system during upper Frio/Anahuac time.

The Frio Formation around Galveston is characterized by complex faulting (fig. 30). Growth faults and associated rollover anticlines are productive in the more updip fields, but production is controlled by a densely faulted, domal structure at Point Bolivar North (figs. 30 and 31). The structural setting at Shipwreck field, which is eastward along strike from Point Bolivar North, was not determined.

Production trends show that fields along the downdip margin of the Houston delta system can be prolific but are often short lived. Point Bolivar North has produced 57.5 million boe, mostly between 1975 and 1981, when production ranged from 20 to almost 60 Bcf of gas/year (fig. 32a). Shipwreck field has had a similar production history (fig. 32b), but it was only about half as long (1977-1980) and has totaled about half as much (25 million boe). Although total amounts are less, Texas City Dike production trends coincide historically with those of Shipwreck (fig. 32c). During production tests in several wells at Point Bolivar North and Shipwreck fields, calculated absolute open flows of 0.25 Bcf of gas/day were reported (Railroad Commission of Texas, Hearing Files). High original pressures and efficient water and pressure-depletion drives permitted the high annual productions. Reservoir compartmentalization by dense faulting and the small number of producing zones (two) resulted in relatively short productive life spans.

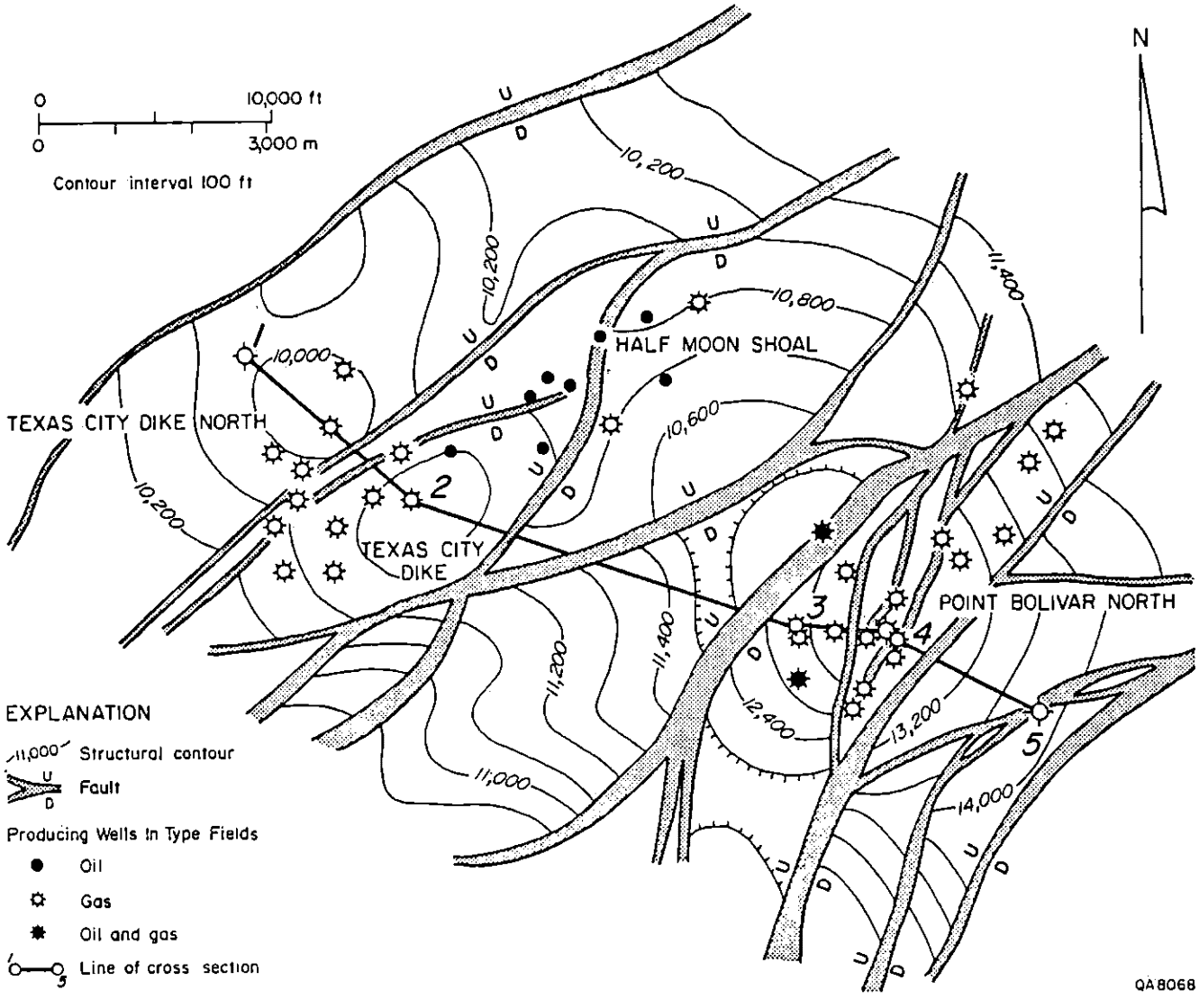

Figure 30. Structural configuration (top of middle Frio) of play IX typical fields exclusive of Shipwreck.

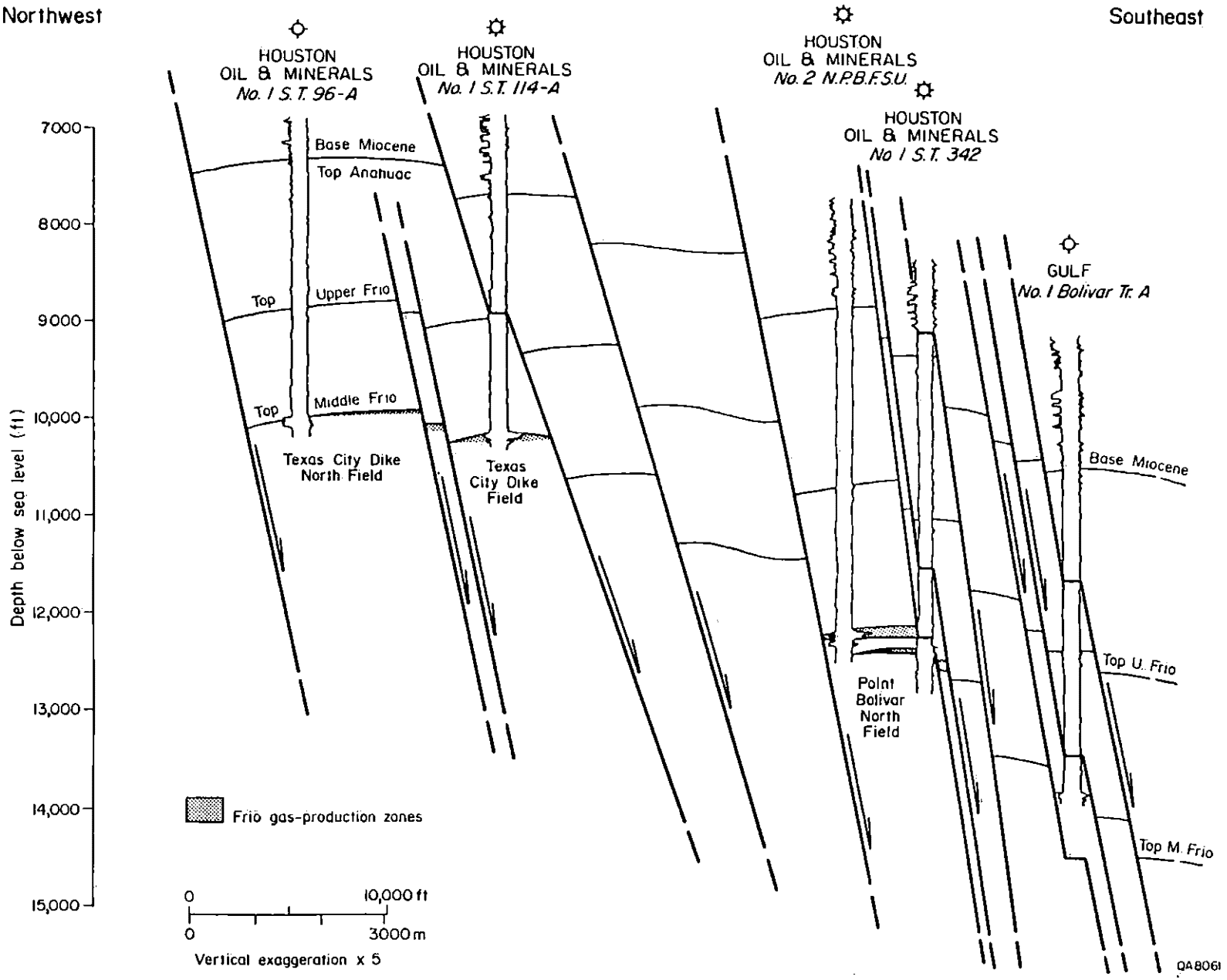

Figure 31. Structural dip cross section through several play IX typical fields. See figures 28 and 30 for location of section line.

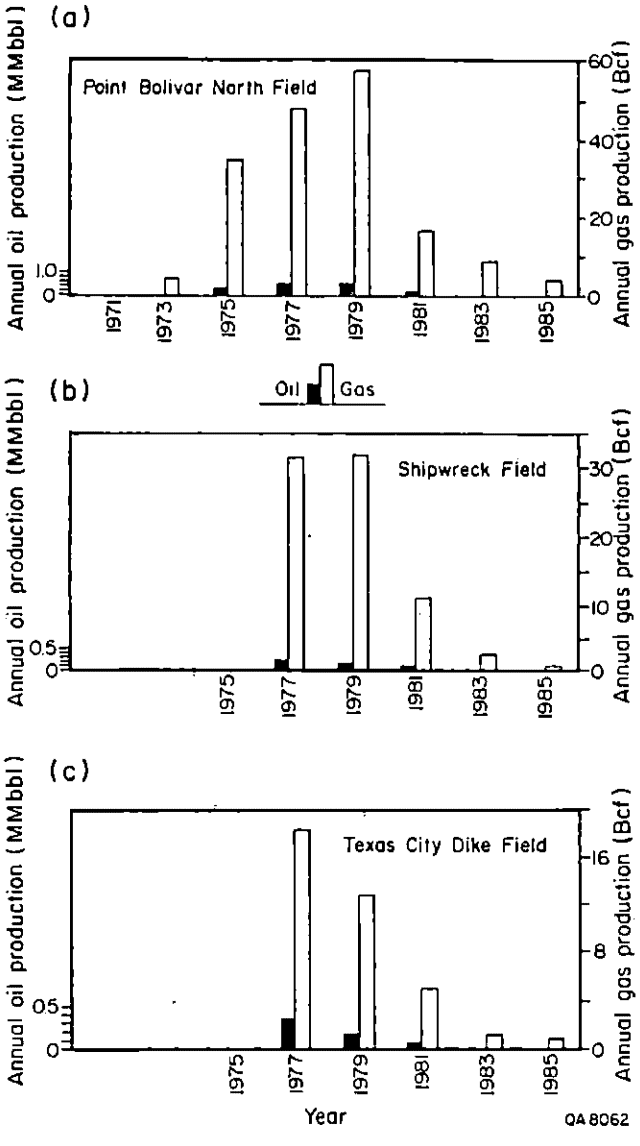

Figure 32. Historical Frio production trends, examples from play IX.

OFFSHORE EXPLORATION POTENTIAL AND PROSPECTIVE FAIRWAYS

Exploration potential of the offshore Frio Formation is determined by the depositional and structural framework (Galloway, 1986), historical production trends, and reservoir conditions. The prime limiting factor is availability of reservoir-quality sandstones. Regional sandstone maps (pl. 3) indicate a low probability of finding permeable Frio sandstone reservoirs in northeastern Matagorda Island, southwestern Brazos, most of High Island, and southern South Padre Island offshore areas. Apparently, these areas are dominated by marine-shelf and slope mudstones. Shelf-edge and intraslope subbasins filled with fault-bounded, resedimented pods of mixed sand, silt, and mudstone may occur in this setting but are speculative, unpredictable targets (Galloway and others, 1982). Onlap slope wedges or gorges similar to the Hackberry of play Xa might also exist along these mud-dominated shelf/slope areas as sand-bearing submarine canyon and fan systems (Ewing and Reed, 1984). Exploratory deep drilling, paleontologic analysis, and seismic stratigraphy might locate such wedges (Galloway and others, 1982).

Frio sandstones have been mapped in the South Padre Island, North Padre Island, Mustang Island, southwestern Matagorda Island, northeastern Brazos, Galveston, and southwestern High Island offshore areas (pl. 3). Offshore Frio sandstone facies are mainly deltaic and delta-margin deposits, and their downdip limits at depth have not been definitely outlined by drilling. Sandstone distribution is the main criterion for selecting and outlining prospective exploration fairways (fig. 33).

Fairway 1 reservoirs are deep (10,000 to >15,000 ft [3,050 to >4,575 m]), distal delta-front sandstones in the northeastern Galveston offshore area (fig. 33). A single sand-rich sequence, containing up to 150 ft (46 m) of reservoir-quality sandstone, is continuous throughout fairway 1. Shipwreck field (cumulative

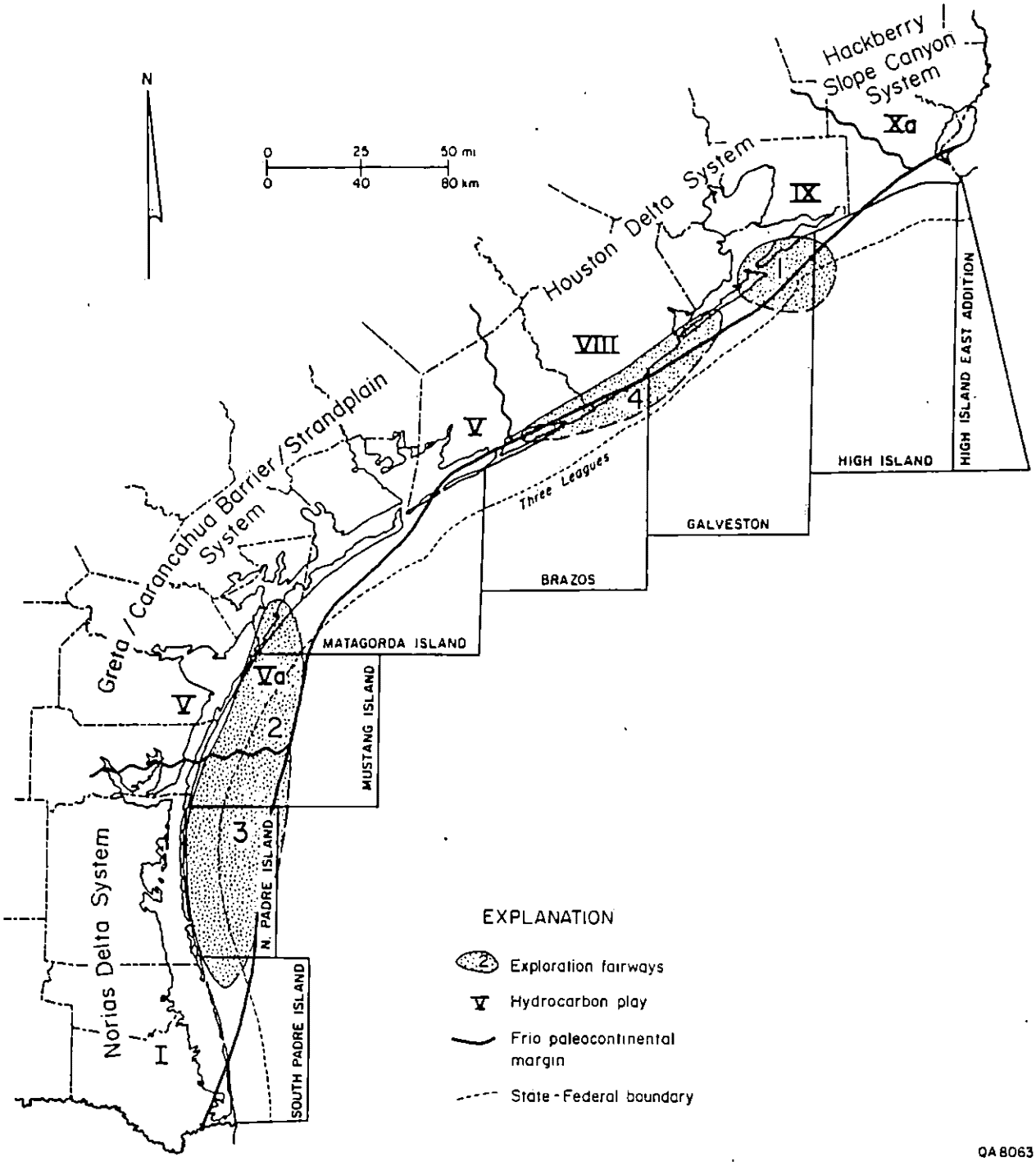

Figure 33. Offshore Frio prospective fairways of optimal exploration potential. Distribution of distal Frio major depositional systems and plays are also shown.

production of 146 Bcf of gas), located in State waters at the center of fairway 1, produces from 40 ft (12 m) of sandstone. However, the much smaller Caplen South field (5.85 Bcf of gas), located in the northeastern corner of the Galveston offshore area (pl. 5), produces from 20 ft (6 m) of sandstone and is probably more typical of potential new-field discoveries in fairway 1 in the Federal OCS.

Regional trends suggest that in fairway 1 porosity and permeability are good, temperatures are high, and pressures are variable. All Frio reservoirs in fairway 1, however, are at least transitionally geopressured. Temperatures range from 200°F to 300°F. A complex structural setting with abundant traps in faulted anticlines and domes indicates that numerous new discoveries are possible in fairway 1. Production trends suggest that future discoveries could yield 10 to 300 Bcf of gas during relatively short (5 to 10 years) productive life spans.

Fairway 2 reservoirs are the distal shoreface/shelf and reworked delta-fringe sandstones of play Va, located in Mustang Island and southwestern Matagorda Island offshore areas (fig. 33). A thick sequence of upper and middle Frio mudstone with numerous interbedded sand-rich zones occurs between about 8,000 and 15,000 ft (2,439 and 4,575 m). Although adjacent Frio fields onshore produce from as many as 10 sand-rich zones (for example, Mustang Island field), offshore fields in fairway 2 currently contain one to three producing horizons. However, as in fairway 1, a single reservoir in fairway 2 can be prolific (for example, Samedan field, where cumulative production from one zone was 114 Bcf of gas in 6 years). Most offshore Frio fields are in fairway 2 (play Va and adjacent parts of play V, pl. 5), which also includes more Federal OCS area than does fairway 1 (fig. 33), although no Frio discoveries have yet been made in the OCS.

Regional trends and studies of typical fields suggest that reservoir conditions and structural setting are favorable in fairway 2. Sandstone porosity and

permeability are best developed between 8,000 and 11,000 ft (2,439 and 3,354 m), where temperatures range from 160°F to 260°F and pore fluids are hydropressured to geopressured. The structural setting in fairway 2, although simpler than that in fairway 1, includes a variety of trap-forming faults, anticlines, and domes. Production trends in fairway 2 are similar to those in fairway 1, although, since 1969, more big discoveries have been made in fairway 1 (Point Bolivar North, Texas City Dike, Shipwreck) than in fairway 2 (only Samedan).

Fairway 3 contains a thick sequence of proximal to distal deltaic sandstones (play I) in North Padre Island and southern Mustang Island offshore areas (fig. 33). From 9,000 to 16,000 ft (2,745 to 4,880 m) or deeper, fairway 3 has a high net sandstone, but average reservoir quality is probably poor. However, density of drilling is low, and regional reservoir-quality trends do not always reflect local porosity/permeability conditions. Fairway 3 includes a large OCS area that covers most of the North Padre Island Area and part of the Mustang Island Area (fig. 33). The few existing offshore fields in fairway 3 are in the southern part of Mustang Island Area (Sprint South [35 Bcf of gas] and the smaller Block 978-S and Block 881-L fields, pl. 5). Based on historical trends and reservoir-quality data, exploration potential of fairway 3 should be greatest in the Mustang Island offshore area. Temperatures increase toward the south, and pressures increase northward. The structural setting is similar to that in the adjacent fairway 2.

Fairway 4 includes very deep (>13,000 ft [>3,960 m]), distal delta-front and upper-slope sandstones of the middle and lower Frio as well as isolated strike-aligned sandstones of the upper Frio (9,000 to 13,000 ft [2,745 to 3,960 m]) in Brazos and Galveston offshore areas (fig. 33). The upper Frio sandstones are apparently transgressive, having been reworked along the shelf margin from older deltaic deposits. Reservoir quality, temperature/pressure conditions, and structural

setting are probably similar to those in nearby fairway 1. However, fairway 4 reservoirs may not extend into the Federal OCS (fig. 33). No offshore Frio discoveries have yet been made in fairway 4.

In terms of exploration favorability in the OCS, fairways 1 and 2 are about equally good and include the most prospective OCS areas for Frio discoveries. In fairway 3, OCS exploration potential is greatest in the north, adjacent to fairway 2. Fairway 4 has good Frio exploration potential in State waters but only moderate to poor potential in the adjacent OCS. Deep Frio offshore discoveries in all fairways will probably be dry-gas-dominated, short-lived fields with annual productions ranging widely from 1 to 100 Bcf. Among new-field discoveries, many more will be smaller than larger.

Even with the refinement of the depositional systems approach in interpreting and predicting reservoir characteristics, the downdip extent of productive sandstones in Texas Gulf Coast Tertiary formations was relatively unexpected. Deep discoveries in the distal parts of the onshore Wilcox and Yegua extended the known sand-bearing parts of those formations beyond previously predicted limits. Deep drilling in the offshore Federal OCS area might reveal sandy Frio intervals many miles seaward of the 3-league boundary.

CONCLUSIONS

In the Federal OCS, distal Frio exploration should be most successful in Mustang Island (fairway 2) and northeastern Galveston (fairway 1) offshore areas, where sandstones display good reservoir quality. Fields are most numerous and production has been greatest along the Coastal Zone adjacent to Mustang Island and Galveston offshore areas. In the Mustang Island Area, deep Frio gas fields might be found 15 mi (24 km) or more seaward of the 3-league line. In the Galveston Area, favorable reservoir sandstones may extend 5 to 10 mi

(8 to 16 km) into the OCS. These OCS areas contain thin, deep (>10,000 ft [>3,049 m]), high-pressured, high-temperature gas reservoirs capable of yielding up to 100 Bcf of gas annually for as long as 10 years, although less prolific reservoirs are much more common. The North Padre Island area OCS also has deep Frio potential. State-owned offshore areas adjacent to the OCS areas just cited have equal or better Frio potential. In addition, Frio exploration potential exists in the State offshore in northern South Padre Island Area, southwestern Matagorda Island Area, northeastern Brazos Area, and most of the Galveston Area.

Distal Frio net sandstone is thickest in North Padre, Mustang Island, and Galveston offshore areas. Across the Texas Coastal Zone and shelf, reservoir quality increases regionally northeastward, but local conditions vary. Measured porosities and permeabilities in selected fields are highest in the Mustang Island offshore area. Reservoir quality generally should be best in a thick zone of transition from hydropressured to geopressured conditions. Most of the Frio Formation offshore is at least transitionally geopressured.

ACKNOWLEDGMENTS

This research was supported by the Minerals Management Service, U.S. Department of the Interior, under agreement no. 14-12-0001-30296. Steven J. Seni guided research procedure and progress. Research assistant Timothy G. Walter helped prepare illustrations. Comments by reviewers Steven J. Seni, Noel Tyler, and Jules R. DuBar improved the clarity and content of this manuscript. Word processing was by Kurt Johnson, under the supervision of Lucille C. Harrell. Drafting was by Marty Thompson, under the supervision of Richard L. Dillon. Editing was by Duran Dodson. The author's appreciation is extended to all who contributed to the preparation of this report.

REFERENCES

Berg, R. R., and Powell, R. R., 1976, Density-flow origin for Frio reservoir sandstones, Nine Mile Point field, Aransas County, Texas: Gulf Coast Association of Geological Societies Transactions, v. 26, p. 310-319.

Ewing, T. E., and Reed, R. S., 1984, Depositional systems and structural controls of Hackberry sandstone reservoirs in Southeast Texas: The University of Texas at Austin, Bureau of Economic Geology Geological Circular 84-7, 48 p.

Galloway, W. E., 1986, Depositional and structural framework of the distal Frio Formation, Texas Coastal Zone and shelf: The University of Texas at Austin, Bureau of Economic Geology Geological Circular 86-8, 16 p.

Galloway, W. E., Hobday, D. K., and Magara, K., 1982, Frio Formation of the Texas Gulf Coast Basin--depositional systems, structural framework, and hydrocarbon origin, migration, distribution, and exploration potential: The University of Texas at Austin, Bureau of Economic Geology Report of Investigations No. 122, 78 p.

Gardner, G. H. F., Gardner, L. W., and Gregory, A. R., 1974, Formation velocity and density--the diagnostic basics of stratigraphic traps: Geophysics, v. 39, p. 770-780.

Gregory, A. R., 1977, Aspects of rock physics from laboratory and log data that are important to seismic interpretation, in Payton, C. E., ed., Seismic stratigraphy--applications to hydrocarbon exploration: American Association of Petroleum Geologists Memoir 26, p. 15-46.

Gregory, A. R., Dodge, M. M., Posey, J. S., and Morton, R. A., 1980, Volume and accessibility of entrained (solution) methane in deep geopressured reservoirs--Tertiary formations of the Texas Gulf Coast: The University of Texas at Austin, Bureau of Economic Geology, report prepared for the U.S. Department of Energy, Division of Geothermal Energy, under contract no. DE-AC08-78ET11397, 390 p.

Hicks, T. E., 1952, Mustang Island field, Nueces County, Texas: Gulf Coast Association of Geological Societies Transactions, v. 2, p. 42-61.

Jones, P. H., 1975, Geothermal and hydrocarbon regimes, northern Gulf of Mexico Basin, in Dorfman, M. H., and Deller, R. W., eds., First geopressured geothermal energy conference: The University of Texas at Austin, Center for Energy Studies, Proceedings, p. 15-97.

Kehle, R. O., 1971, Geothermal survey of North America, 1971 progress report: Research Committee, American Association of Petroleum Geologists, unpublished, 31 p.

Kling, Don, compiler, 1972, Type logs of South Texas fields 1972, volume 1--Frio trend: Corpus Christi Geological Society, p. 84 and 100.

Lewis, C. R., and Rose, S. C., 1970, A theory relating high temperatures and overpressures: Journal of Petroleum Technology, v. 22, p. 11-16.

Loucks, R. G., Dodge, M. M., and Galloway, W. E., 1984, Regional controls on diagenesis and reservoir quality in lower Tertiary sandstones along the Texas Gulf Coast, in McDonald, D. A., and Surdam, R. C., eds., Clastic diagenesis: American Association of Petroleum Geologists Memoir 37, p. 15-45.

_____ 1986, Controls on porosity and permeability of hydrocarbon reservoirs in lower Tertiary sandstones along the Texas Gulf Coast: The University of Texas at Austin, Bureau of Economic Geology Report of Investigations No. 149, 78 p.

Morton, R. A., and Land, L. S., 1987, Regional variations in formation water chemistry, Frio Formation (Oligocene), Texas Gulf Coast: American Association of Petroleum Geologists Bulletin, v. 71, no. 2, p. 191-206.

Mulle, G. E., 1967, Murdock Pass field, Kenedy County, Texas, in Typical oil and gas fields of South Texas: Corpus Christi Geological Society, p. 129-131.

Reynolds, M. B., and Reese, D. L., 1967, Chevron field offshore Kleberg County, Texas, in Typical oil and gas fields of South Texas: Corpus Christi Geological Society, p. 43-49.

Weise, B. R., Edwards, M. B., Gregory, A. R., Hamlin, H. S., Jirik, L. A., and Morton, R. A., 1981, Geologic studies of geopressured and hydropressured zones in Texas: test-well site selection: The University of Texas at Austin, Bureau of Economic Geology, report prepared for Gas Research Institute under contract no. 5011-321-0125, 308 p.

APPENDIX A. Deep wells used for Galloway's (1986) distal Frio study.

Plate 1 ID No.	County or Offshore Area	Operator	Lease or Block	Total Depth (ft)
1	Jefferson	Texaco	#1 Port Arthur Refinery Fee	14,200
2	Jefferson	Humble	#1 St. Tr. 38	13,900
3	Chambers	MRT Expl.	#1 Barrow Ranch	11,650
4	Jefferson	Shell	#2 McFaddin Fee Cross	14,825
5	Jefferson	Magnolia	#1-A McFaddin Trust	15,005
6	Jefferson	D. D. Feldman	#1 B. E. Quinn	11,520
7	Jefferson	Austral	#B-1 M. Fowler	10,517
8	Jefferson	Pan American	#1 J. T. White et al.	16,000
9	Jefferson	Mecom & Blairsville	#1 Hennessy	11,008
10	Jefferson	San Juan Expl.	#1 F. M. Hebert	11,145
11	Orange	Prairie Prod.	#1 E. Brown	8,515
12	Orange	Anderson & Bowman	#1 Lutcher-Moore Lumber	10,817
13	Chambers	Belco	#1 Crawford 159	13,110
14	Jefferson	Belco	#2 Crawford 161	14,526
15	Chambers	J. W. Mecom	#1 T. Middleton et al.	12,600
16	Brazoria	Phillips Petroleum	#1 St. Tr. 32	16,500
17	Galveston	Houston O & M	#1 Block 182-S	12,540
18	Galveston	Houston O & M	#1 Block 151-S	12,200
19	Galveston	Rutherford	#1 Block 315-S	12,000
20	Brazoria	Texaco	#1 Tarpon Mound	15,236
21	Galveston	McCulloch	#1 Lobit Unit	18,463
22	Galveston	Dorchester	#1 University of Texas	10,979
23	Galveston	Brewster-Bartle	#1-A St. Tr. 100-A	11,735
24	Galveston	Gulf	#1 Federal Pelican	13,383
25	Galveston	Gulf	#1 Bolivar Tract "A"	14,002
26	Galveston	Gulf	#1 St. Tr. 315	16,031
27	Galveston	Humble	#A-133 St. Tr. 199	13,512
28	Galveston	Eason-Braun-Chambers	#1 St. Tr. 160	11,521
29	Chambers	Humble	#1 G. C. Jackson	14,100
30	Brazoria	Phillips	#1-S Houston Farms	15,000
31	Galveston	Pan American	#1 Stewart Title & Guaranty	14,786
32	Chambers	Phillips	#1-A Daw	13,150
33	Galveston	Sun & Phillips	#1 St. Tr. 175	9,446
34	Galveston	Mosbacher-Transco	#1 St. Tr. 146	11,800
35	Galveston	Pan American	#1 Maco Stewart Comm.	10,606
36	Galveston	Rutherford	#1 St. Tr. 324	11,000
37	Galveston	Shell & Texas Co.	#1 St. Tr. 195	11,775
38	Galveston	Brewster-Bartle	#1 St. Tr. 99-A	10,712
39	Brazoria	Union Oil Calif.	#1 Houston Farms	15,000
40	Galveston	Mesa	#1 Block 100-L	12,968
41	Galveston	Humble	#1 St. Tr. 151	11,200
42	Galveston	Mitchell Energy	#1 Block 171-S	13,902
43	Galveston	Houston O & M	#1 St. Tr. 232	11,900
44	Galveston	Sun	#10 Cade Est.	12,500
45	Chambers	McMoran	#1 St. Tr. 64	11,890
46	Galveston	Houston O & M	#1 St. Tr. 342	12,900

APPENDIX A (cont.)

Plate 1 ID No.	County or Offshore Area	Operator	Lease or Block	Total Depth (ft)
47	Galveston	Russell Maguire	#1 E. Taylor	11,107
48	Galveston	Cities Service	#1 Weidmann	9,810
49	Galveston	Humble	#1 St. Tr. 81	16,701
50	Brazoria	Phillips	#2 Houston "M"	18,006
51	Brazoria	Phillips	#1 Houston "JJ"	17,018
52	Galveston	Texaco	#1 St. Tr. 319	13,720
53	Chambers	Pan American	#1 Kieke	11,150
54	Chambers	Sundance	#1 Mays Est.	10,378
55	Chambers	Placid	#1 Canada	12,512
56	Brazoria	General Crude	#1 Shell Point	16,510
57	Brazoria	Sun	#1 Houston Farms	17,980
58	Brazoria	General Crude	#2 Alligator Point	13,340
59	Brazoria	Phillips	#1 Houston "BB"	16,004
60	Brazoria	General Crude	#3 Alligator Point	11,495
61	Brazoria	Gulf	#1 St. Tr. 8	14,685
62	Brazoria	General Crude	#1 Alligator Point	12,420
63	Galveston	Mobil	#1 Halls Bayou Ranch	18,990
64	Galveston	Pure	#1 Houston Farms	17,052
65	Galveston	Pure	#B-1 Houston Farms	12,298
66	Galveston	Gulf	#1 Emil Firth Est.	13,824
67	Galveston	Sun	#1 Vangemann	15,002
68	Galveston	E. L. Cox	#1 Halls Bayou Ranch	14,986
69	Galveston	Davis	#1 Pierce Educational Fund	11,654
70	Galveston	Inexco	#1 University of Texas	11,025
71	Galveston	Humble	#1 W. Ostermeyer	18,988
72	Matagorda	Superior	#1 Robbins Est.	18,500
73	Matagorda	Standard Texas	#1 M. H. Lewis et al.	9,664
74	Matagorda	Magnolia	#2 J. Hawkins	16,003
75	Matagorda	Stanolind et al.	#1 R. Sanborn	15,012
76	Matagorda	Stanolind et al.	#1 M. C. Fall	16,015
77	Matagorda	Gulf	#1 O. E. Phillips	16,645
78	Brazoria	Phillips	#1 Poole "C"	17,000
79	Brazoria	Union Calif.	#1 Davis	12,975
80	Brazoria	Dow Chemical	#1 J. Bute	13,020
81	Brazoria	Monsanto	#1 Austin	11,600
82	Brazoria	Brazos	#1 Clemens St. Fm. 1-A	11,305
83	Brazoria	Gulf	#1 S. S. Perry	12,984
84	Brazoria	Texaco	#1 Hoskins Mound Fee NCT-1	17,323
85	Brazoria	Humble	#1 R. W. Vieman	15,725
86	Brazoria	Tenneco	#1 American Fletcher	18,300
87	Brazoria	Mobil	#1 Retrieve St. Fm. Tr. 1	13,468
88	Brazoria	Continental	#1 White Frost Unit	18,025
89	Brazoria	Gulf	#1 L. B. Hervey	12,420
90	Brazoria	Humble	#6 Freeport Sulfur	17,695
91	Brazoria	Pan American	#A-1 B.R.L.D.	14,005
92	Brazoria	North American Royalties	#1 Hampil	11,794

APPENDIX A (cont.)

Plate 1 ID No.	County or Offshore Area	Operator	Lease or Block	Total Depth (ft)
93	Matagorda	Phillips	#1-A State "N"	20,500
94	Matagorda	Mobil	#15 E. Cornelius	16,500
95	Matagorda	Socony Mobil	#3 J. Hawkins	18,500
96	Matagorda	Gulf	#1 C. G. Hamill et al.	16,480
97	Matagorda	American Petrofina	#1 D. H. Braman	17,300
98	Matagorda	Magnolia & Sinclair	#1 Le Tulle	17,000
99	Matagorda	Energy Development	#1 D. H. Braman, Jr.	18,545
100	Matagorda	Lear	#1-A Baer Est.	16,235
101	Matagorda	Tennessee Gas	#1 W. Doss	13,492
102	Matagorda	Continental	#1 N. Caldwell	16,040
103	Matagorda	Houston O & M	#1 H. Norris et al.	16,961
104	Matagorda	American Nat. Res.	#1 Baer Ranch	17,010
105	Calhoun	Coastal States & Royal	#1 Duncan	11,509
106	Aransas	Richardson & Bass	#1 St. Tr. 235	11,161
107	Aransas	Richardson & Bass	#1 St. Tr. 265	11,892
108	Matagorda Island	Coastal States	#1 Block 831-S	11,994
109	Matagorda Island	Standard Texas	#1 Block 833-S	11,950
110	Matagorda Island	Standard Texas	#1 Block 835-S	11,828
111	Matagorda Island	Belco	#1 Block 721-L	13,297
112	Matagorda Island	Standard Texas	#1 Block 840-S	12,000
113	Calhoun	Shell	#1 St. Tr. 143	18,500
114	Aransas	Humble	#1 St. Tr. 166	16,000
115	Aransas	Getty	#1 St. Tr. 95	11,478
116	Calhoun	Brown & Skelly	#1 St. Tr. 33	10,006
117	Calhoun	Western Nat. Gas	#1 St. Tr. 55	11,548
118	Calhoun	G. R. Brown	#1 St. Tr. 81	12,510
119	Calhoun	Southern Union	#1 St. Tr. 118	10,000
120	Calhoun	Texaco	#1 St. Tr. 186	10,200
121	Calhoun	H. Hunt	#1 St. Tr. 198	12,009
122	Calhoun	Austral	#1 La Salle Ranch	9,518
123	Calhoun	Humble	#1 D. E. Schicke	12,000
124	Calhoun	Skelly	#1 Austin E. St. Tr. 157	9,300
125	Nueces	Westland	#1 St. Tr. 225	11,524
126	Calhoun	Amerada	#1 E. G. Rosen	10,115
127	Calhoun	Mitchell Energy	#1 St. Tr. 65	8,712
128	Nueces	Standard Texas	#1 St. Tr. 2	10,885
129	Nueces	Shell	#1 St. Tr. 277	13,002
130	Matagorda	Magnolia	#1 W. W. Rugeley	16,510
131	Palacios	Pan American	#1 Silver Lake Ranch	16,000
132	Calhoun	Walter Van Norman	#1 La Salle Ranch	16,000
133	Calhoun	Glasscock et al.	#1 St. Tr. 131	11,005

APPENDIX A (cont.)

Plate 1 ID No.	County or Offshore Area	Operator	Lease or Block	Total Depth (ft)
134	Calhoun	Tennessee Gas	#1 C. H. Stiernberg	13,009
135	Aransas	Continental	#46 St. Charles Ranch	12,826
136	Aransas	Western Natural Gas	#9 St. Charles	12,020
137	Aransas	Alcoa	#1 St. Tr. 19	11,510
138	San Patricio	Tenneco	#1 W. G. McCampbell	14,037
139	Nueces	McMoran	#1 St. Tr. 312	15,407
140	Matagorda	Brazos	#2 Savage	16,007
141	Matagorda	Pan American	#A-2 Silver Lake Ranch	13,037
142	Matagorda	Pennzoil	#1 St. Tr. 195	14,072
143	Matagorda	McCulloch	#1 City of Palacios	15,991
144	Matagorda	Duer Wagner	#1 Palacios Airport	13,889
145	Matagorda	Exxon	#1-A Le Tulle Green	14,512
146	Mustang Island	McMoran	#1 Block 985-S	10,067
147	Mustang Island	Pan American	#1 Block 981-S	10,826
148	Kleberg	Sun	#1-A Dunn-McCampbell	11,018
149	Mustang Island	Amoco	#1 Block 979-S	8,200
150	Mustang Island	Cherryville	#1 Block 978-S	13,350
151	Mustang Island	Sun	#1-A Block 976-S	9,234
152	Kleberg	Sun	#A-2 Dunn-McCampbell	8,412
153	Mustang Island	Sun	#A-1 Block 975-S	9,319
154	Mustang Island	Sun	#1 Block 974-S	14,042
155	Mustang Island	Standard Texas	#15 Block 954-S	9,500
156	Mustang Island	Standard Texas	#63 Block 954-S	9,462
157	Mustang Island	Standard Texas	#98 Block 952-S	9,042
158	Mustang Island	Standard Texas	#36 Block 952-S	9,086
159	Mustang Island	Standard Texas	#22 Block 951-S	8,614
160	Mustang Island	Standard Texas	#87 Block 949-S	10,126
161	Mustang Island	Standard Texas	#53 Block 952-S	8,712
162	Mustang Island	Standard Texas	#53 Block 948-S	9,975
163	Mustang Island	Standard Texas	#28 Block 947-S	10,201
164	Mustang Island	Standard Texas	#24 Block 953-S	9,053

APPENDIX A (cont.)

Plate 1 ID No.	County or Offshore Area	Operator	Lease or Block	Total Depth (ft)
165	Mustang Island	Texaco	#1 Block 946-S	11,000
166	Mustang Island	Humble	#A-1 Block 819-L	10,500
167	Mustang Island	Sun	#2 Block 938-S	9,550
168	Mustang Island	Sun	#1 Block 937-S	8,991
169	Mustang Island	Standard Texas	#58 Block 932-S	11,510
170	Mustang Island	McMoran	#2 Block 924-S	10,287
171	Mustang Island	Gulf	#1 Block 818-L	14,432
172	Mustang Island	Samedan	#1 Block 841-L	9,536
173	Mustang Island	Gulf	#1 Block 842-L	15,530
174	Mustang Island	Union Calif.	#1 Block 842-L	14,273
175	Mustang Island	Mobil	#1 Block 859-L	12,016
176	Nueces	Socony Mobil	#1 Burton-Dunn	12,020
177	Nueces	Arkansas Fuel	#B-1 S. E. Wilson	8,950
178	Mustang Island	Louisiana Land & Expl.	#1 Block 921-S	10,816
179	Mustang Island	Cities Service	#2-A Block 796-L	10,556
180	Mustang Island	Samedan	#1 Block 817-L	10,196
181	Mustang Island	Inexco	#1 Block 797-L	12,226
182	Mustang Island	Cities Service	#1 Block 795-L	12,505
183	Mustang Island	C & K Offshore	#1 Block 920-S	13,768
184	Mustang Island	Arkansas Fuel	#1 Block 905-S	12,250
185	Mustang Island	Arkansas Fuel	#1 Block 910-S	9,190
186	Mustang Island	Arkansas Fuel	#1 Block 911-S	8,877
187	Mustang Island	Arkansas Fuel	#1 Block 904-S	9,372
188	Mustang Island	McMoran	#1-A Block 906-S	8,976

APPENDIX A (cont.)

Plate 1 ID No.	County or Offshore Area	Operator	Lease or Block	Total Depth (ft)
189	Mustang Island	McMoran-Transco	#2 Block 901-S	8,851
190	Mustang Island	Texaco	#1 Block 903-S	8,400
191	Mustang Island	Cities Service	#1 Block 773-L	14,496
192	Mustang Island	Cabot	#1 Block 773-L	8,149
193	Mustang Island	Texas Gas Expl.	#1 Block 773-L	14,338
194	Mustang Island	Shell	#1 Block 899-S	12,667
195	Mustang Island	Shell	#1 Block 896-S	13,660
196	Mustang Island	Zapata and C & K	#3 Block 773-L	8,322
197	Mustang Island	Gulf	#1 Block 898-S	10,335
198	Mustang Island	Gulf-Humble-Shell	#B-1 Block 772-L	14,105
199	Mustang Island	Gulf	#1 Block 773-L	13,668
200	Mustang Island	Patrick	#1 Block 774-L	14,442
201	Mustang Island	Gulf	#1 Block 774-L	12,500
202	Mustang Island	Union Calif.	#1 Block 775-L	14,025
203	Mustang Island	Humble	#1 Block 772-L	12,661
204	Mustang Island	Gulf-Sun-Seaboard	#A-3 Block 889-S	13,505
205	Mustang Island	Gulf-Seaboard-Sun	#A-2 Block 889-S	12,765
206	Mustang Island	Shell	#1 Block 888-S	12,027
207	Mustang Island	Shell	#1 Block 891-S	13,999
208	Mustang Island	Sun	#1 Block 883-S	13,001
209	Mustang Island	Sun & Seaboard	#1-B Block 882-S	14,206
210	Mustang Island	Shell	#1 Block 884-S	13,444
211	Mustang Island	Shell	#1 Block 885-S	12,299

APPENDIX A (cont.)

Plate 1 ID No.	County or Offshore Area	Operator	Lease or Block	Total Depth (ft)
212	Mustang Island	Southland Royalty	#1 Block 886-S	11,600
213	Mustang Island	Cherryville	#1 Block 886-S	9,484
214	Nueces	Atlantic Ref. et al.	#1 S. E. Wilson, Jr.	11,505
215	Mustang Island	Arkansas Fuel	#1 Block 880-S	11,056
216	Nueces	Arkansas Fuel et al.	#C-1 S. E. Wilson	8,363
217	Nueces	Pure	#1 S. E. Little	8,961
218	Nueces	Panhandle	#1 Grant et al.	9,009
219	Mustang Island	Occidental	#2 Block 749-L	11,699
220	Mustang Island	Occidental & Signal	#1 Block 749-L	13,131
221	Mustang Island	Atlantic Ref.	#1 Block 726-L	12,034
222	Nueces	Cherryville	#1 Burton-Dunn	15,045
223	Mustang Island	Samedan	#G-1 Block 818-L	11,015
224	Kleberg	Shell	#1 St. Tr. 206	10,501
225	Kleberg	Samedan	#2 Jones	10,570
226	Nueces	Humble	#1 St. Tr. 173	11,000
227	Nueces	Centennial Royalty	#1 F. J. Smith	11,400
228	Nueces	Marion	#1 Peterson	15,916
229	Nueces	Getty	#1 St. Tr. 41	12,370
230	Nueces	Kilroy et al.	#1 St. Tr. 83	10,312
231	Nueces	Atlantic Richfield	#1 St. Tr. 454	12,500
232	Nueces	Tenneco	#1 St. Tr. 458	12,000
233	Nueces	La Gloria et al.	#1 St. Tr. 334	8,850
234	Nueces	Monday	#1 E. Walsh	7,503
235	Nueces	Humble	#1 Oso, St. Tr. C	8,837
236	Kleberg	Exxon	#2 St. Tr. 143	7,700
237	Kleberg	Texaco	#1 St. Tr. 187	10,000
238	Kleberg	Humble	#1 St. Tr. 196	11,505
239	Kleberg	Humble	#1 St. Tr. 197	16,000
240	Kleberg	Humble	#3 King Rch-Ojo de Agua	8,457
241	Kleberg	Humble	#1 King Rch-Ojo de Agua	11,000
242	Nueces	Sinclair	#1 St. Tr. 401	8,150
243	San Patricio	L. E. Hoover et al.	#1 M. W. Hogg et al.	9,215
244	Kenedy	Sun	#1 St. Tr. 218	8,380
245	Kenedy	Kilroy & American Quasar	#2 Kenedy Ranch	7,512
246	Kleberg	Humble	#1 St. Tr. 25	9,912
247	Nueces	Humble	#F-2 St. Tr. 31	9,298
248	Mustang Island	Union Calif.	#1 Block 859-L	14,665
249	Mustang Island	Exxon	#1 Block 1003-S	13,002

APPENDIX A (cont.)

Plate 1 ID No.	County or Offshore Area	Operator	Lease or Block	Total Depth (ft)
250	Mustang Island	McMoran	#2 Block 858-L	16,700
251	Mustang Island	McMoran	#3 Block 859-L	15,538
252	Mustang Island	McMoran	#2 Block 859-L	14,650
253	Mustang Island	Gulf	#1 Block 942-S	12,000
254	Mustang Island	Exxon	#1 Block 750-L	12,900
255	Mustang Island	Houston O & M	#1 Block 866-L	12,776
256	Mustang Island	Mobil	#1 Block 799-L	11,240
257	Nueces	Atlantic Ref.	#1 St. Tr. 36	14,502
258	Nueces	Sunray	#2 St. Tr. 461	8,006
259	Nueces	Socony Mobil et al.	#1 E. R. Russell	15,000
260	Kenedy	Humble	#7 Mrs. S. K. East B	10,087
261	Nueces	Pan American	#1 U.S.A.	14,033
262	Nueces	Mobil	#3 Lehman G. U.	11,632
263	Kleberg	Humble	#2 King Rch-Lobo	9,000
264	Kleberg	Humble	#G-18 King Rch-E. Laureles	9,000
265	Kleberg	Humble	#3 King Rch-Alazan	10,476
266	Kleberg	Humble	#179 King Rch-Alazan	9,500
267	Kleberg	Humble	#1 St. Tr. 57	13,752
268	Nueces	Exxon	#1 St. Tr. 62	10,358
269	Nueces	Sun Gas	#12 St. Tr. 423	11,970
270	North Padre Island	Mobil	#1 Block 961-L	18,484
271	North Padre Island	Sun	#1 Block 1048-S	10,633
272	Kenedy	Sun	#2 St. Tr. "A" 232	13,032
273	North Padre Island	Zapata Offshore	#1 Block 1009-S	10,242
274	North Padre Island	Carrl	#1 Block 883-L	9,279
275	North Padre Island	Standard Texas	#1 Block 883-L	13,100
276	Kenedy	Gulf	#1 E. Parral Ranch	11,937
277	Kenedy	Humble	#1 St. Tr. 384	12,000
278	Kenedy	Exxon	#79 Mrs. S. K. East	10,601
279	Kenedy	Humble	#C-1 Mrs. S. K. East	13,388
280	Kenedy	Exxon	#67 Mrs. S. K. East	9,484
281	Kenedy	Union Prod.	#1 St. Tr. 348	17,320
282	Kenedy	Humble	#1 St. Tr. 326	10,000
283	Kenedy	Humble	#30 Mrs. S. K. East	16,000
284	Kenedy	Humble	#D-3 Mrs. S. K. East	10,493

APPENDIX A (cont.)

Plate 1 ID No.	County or Offshore Area	Operator	Lease or Block	Total Depth (ft)
285	Kenedy	North Central	#B-1 Kenedy Ranch	8,461
286	Kenedy	Humble	#G-2 J. G. Kenedy, Jr.	8,001
287	Kenedy	Humble	#3 J. G. Kenedy	7,705
288	North Padre Island	Mobil	#1 Block 1006-S	16,817
289	Willacy	Shoreline	#1 L. Walker	11,016
290	Willacy	Sun	#1 Scott	10,001
291	Cameron	Chevron	#1 J. A. Rodriguez	18,484
292	Willacy	Humble	#1 Sauz Rch-Jardin	12,290
293	Willacy	Humble	#2 W. S. Murphy	10,332
294	Willacy	Humble	#1 Sauz Rch-Tenerias	12,501
295	Cameron	Magnolia	#1 G. Kerlin	17,160
296	Willacy	Humble	#1 Willamar G.U.1	15,972
297	Willacy	Humble	#2 Sauz Rch-Nopal	11,966
298	Willacy	Pan American	#1 de Armendaiz	16,000
299	Cameron	Dow Chemical	#1 Cont'l Fee	13,015
300	North Padre Island	Exxon	#1 Block 922-L	13,220
301	North Padre Island	Shell	#3 Block 897-L	14,500
302	North Padre Island	Shell	#1 Block 897-L	15,000
303	North Padre Island	Mobil & New Mexico	#1 Block 884-L	14,435
304	North Padre Island	Arco	#1 Block 957-L	17,011
305	Kenedy	Humble	#G-1 J. G. Kenedy, Jr.	10,935
306	Kenedy	Pan American	#1 J. G. Kenedy, Jr.	15,606
307	Kenedy	Humble	#1 St. Tr. 249	11,695
308	Kenedy	Humble	#D-1 Mrs. S. K. East	12,000
309	North Padre Island	Mobil	#1 St. Tr. 309	17,000
310	Kenedy	Humble	#2 King Rch-Saltillo	13,000
311	Kenedy	Humble	#2 King Rch-Tio Moya	14,003
312	Kenedy	Humble	#1 King Rch-Tio Moya	12,001
313	Kenedy	Mobil	#1 St. Tr. 406	18,620
314	North Padre Island	Home Pet.	#1 Block 902-L	14,900

APPENDIX B. Hydrocarbon production from the distal Frio Formation listed by field. Only fields >1 million boe are listed (1 boe = 6 Mcf gas).

Hydrocarbon Field	Discovery Date	Prod. Type	Cumulative Prod. to 1/86 Total (Mboe)	Gas (MMcf)	Oil (Mbbl)	Ann. Prod. 1985 Gas (MMcf)	Oil (Mbbl)
PLAY I							
Calandria	52	Gas	14,641	87,303	90	7,095	3
Murdock Pass	52	Gas	33,934	203,544	14	794	7
Murdock Pass, E	64	Gas	2,837	17,022	0	0	0
Murdock Pass, N	68	Gas	6,462	38,769	0	693	0
Penascal	52	Gas	4,247	25,458	4	0	0
Potrero Lopena	52	O/G	2,487	13,089	305	231	15
Potrero Lopena, S	66	Gas	2,530	14,976	34	0	0
Potrero Lopena, SW	77	O/G	1,553	8,955	60	1,017	16
San Jose, S	79	Gas	3,552	21,310	0	3,198	0
Sprint, S	68	Gas	6,422	35,222	552	1,238	0
Tenerias	53	Gas	6,414	38,348	23	494	0
Willamar, W	41	O/G	59,297	153,098	33,781	7,928	542
Total Play I Prod.	--	O&G	144,376	657,094	34,863	22,688	583
PLAY V							
Appling, SE	59	Gas	1,895	10,276	182	464	7
Aransas Pass	36	Oil	20,707	951	20,548	34	21
Aransas Pass, E	54	O/G	2,297	9,482	717	74	14
Baer Ranch	65	Gas	2,131	12,785	122	0	0
Bartell Pass	70	Gas	1,216	6,679	103	630	11
Bina	76	Gas	1,319	7,701	35	128	0
Bina, NE	82	Gas	2,568	15,342	11	4,643	0
Bird Island	38	O/G	4,433	15,619	1,830	821	63
Bird Island, SW	61	Gas	1,111	6,465	33	0	0
Burgentine Lake	66	O/G	5,575	26,482	1,161	42	0
Burgentine Lake, SW	67	O/G	3,164	10,890	1,349	0	0
Caney	59	O/G	1,318	2,220	948	1	4
Cayo del Oso	53	Oil	1,561	34	1,555	0	1
Chevron	54	O/G	28,011	145,835	3,705	8	0
Copano Bay, S	62	O/G	19,377	83,574	5,448	967	35
Copano Bay, SW	67	Gas	1,163	5,050	321	0	0
Corpus Channel, NW	56	O/G	11,417	67,632	145	205	19
Corpus Christi, E	53	Gas	11,554	69,098	38	142	0
Corpus Christi Bay, W	61	Gas	6,423	38,321	36	277	3
Dunn-McCampbell	61	Gas	6,567	39,278	21	0	0
Encinal Channel	65	Gas	25,199	147,240	659	1,506	0
Encinal Channel, SE	67	Gas	2,624	14,566	196	89	0
Enos Cooper	53	O/G	3,330	11,205	1,462	4	0
Estes Cove	68	O/G	3,086	6,093	1,055	84	64
Flour Bluff	36	O/G	20,998	6,325	19,944	1,616	181
Flour Bluff, E	40	O/G	40,351	188,717	8,898	2,399	4
Four Corners	77	Gas	2,142	10,824	338	229	4
Fulton Beach	47	O/G	39,439	105,941	21,782	370	17
Fulton Beach, E	52	O/G	3,910	6,928	2,755	0	0
Fulton Beach, N	53	Oil	4,097	1,478	3,851	45	7

PLAY V continued on next page

APPENDIX B (cont.)

Hydrocarbon Field	Discovery Date	Prod. Type	Total (Mboe)	Gas (MMcf)	Oil (Mbbl)	Gas (MMcf)	Oil (Mbbl)
PLAY V (cont.)							
Fulton Beach, W	51	O/G	27,526	111,486	8,945	236	29
Geronimo	58	Gas	3,453	19,001	286	152	2
Goose Island	53	O/G	1,189	3,080	676	36	28
Gregory, E	60	Gas	1,319	5,397	419	52	6
Harvey	50	O/G	3,190	11,200	1,323	29	15
Headquarters	56	Gas	9,549	52,600	782	308	7
Indian Point	56	O/G	10,026	53,224	1,155	229	4
Laguna Larga	49	Gas	74,661	439,326	1,440	12,392	0
Lamar	29	Oil	1,169	1,828	864	1	4
Long Mott, S	51	Gas	1,488	7,817	185	11	0
Magnolia Beach	50	O/G	1,862	5,848	888	78	0
Mag. Beach-Kellers Bay	52	O/G	23,630	124,368	2,909	1,232	0
McCampbell	69	O/G	1,511	4,890	696	74	13
Mudflats	49	O/G	1,292	2,923	805	32	2
Mustang Island	49	O/G	36,911	26,244	32,537	555	54
Mustang Island, W	66	O/G	8,023	43,822	719	302	10
Nine Mile Point	65	Gas	10,878	65,258	2	2,622	0
Nine Mile Point, W	77	O/G	1,126	3,100	609	46	20
Padre, N	72	O/G	3,129	17,471	217	301	10
Palacios	37	O/G	6,682	11,224	4,811	658	50
Panther Reef	57	Gas	3,484	20,792	18	52	0
Panther Reef, N	64	Gas	2,026	11,209	158	0	0
Panther Reef, SW	64	Gas	4,972	29,831	0	1,262	0
Petrucha	62	Gas	2,817	14,897	334	46	1
Pita Island	64	Gas	3,587	21,523	0	624	0
Portland, W	56	O/G	3,919	17,240	1,046	49	16
Puerto Bay	53	O/G	1,216	156	1,190	74	1
Redfish Bay	50	O/G	29,296	62,833	18,824	668	64
Redfish Bay, N	59	O/G	6,764	35,694	815	451	14
Rockport, W	54	O/G	1,730	4,488	982	184	3
Rugeley, SW	77	Gas	7,444	32,625	2,006	2,607	122
Saint Charles, N	52	O/G	1,673	6,458	597	0	0
Salt Lake	48	Oil	2,087	684	1,973	0	0
Stedman Island	51	Gas	8,947	52,987	116	1,184	57
Sweeney	58	Gas	11,999	65,112	1,147	324	3
Virginia	50	O/G	7,762	21,822	4,125	188	29
Wadworth	51	O/G	15,873	74,621	3,436	785	84
Wadworth, S	61	Gas	2,943	15,047	435	4,145	85
Total Play V Prod.	--	O&G	626,136	2,571,157	196,718	46,767	1,188
PLAY Va							
Block 749	74	Gas	4,534	24,160	507	95	0
GOM-ST-904	57	Gas	15,854	90,323	800	508	9
Mustang Isl. Blk. 883	73	Gas	6,661	39,815	25	66	1
Mustang Isl. Blk. 889	55	Gas	3,007	15,486	426	663	13
Samedan	79	Gas	19,037	114,221	0	13,689	0
Total Play Va Prod.	--	O&G	49,093	284,005	1,758	15,021	23

APPENDIX B (cont.)

Hydrocarbon Field	Discovery Date	Prod. Type	Total (Mboe)	Gas (MMcf)	Oil (Mbbl)	Gas (MMcf)	Oil (Mbbl)
PLAY VIII							
Clemens, N	63	Gas	14,628	83,680	681	865	2
Clemens, SW	72	Gas	4,931	27,214	395	429	2
Peach Point, S	76	Gas	5,296	30,683	182	2,948	12
Perry Landing	62	Gas	5,302	31,083	121	0	0
Total Play VIII Prod.	--	O&G	30,157	172,660	1,379	4,242	16
PLAY IX							
Alligator Point	62	Gas	1,990	10,447	249	149	4
Alta Loma	40	O/G	3,658	7,620	2,388	0	0
Alta Loma, E	57	Gas	4,824	23,908	839	0	0
Alta Loma, S	53	O/G	1,878	1,746	1,587	83	99
Alta Loma, W	56	O/G	7,091	34,847	1,283	83	17
Angelina	67	Gas	15,751	75,643	3,144	4,653	72
Big Hill, N	49	Gas	2,648	15,796	15	0	0
Big Hill, NW	61	O/G	2,087	9,504	503	967	16
Caplen, S	75	Gas	1,109	5,837	136	198	2
Chocolate Bayou, S	60	Gas	11,592	59,507	1,674	2,494	70
Dickinson	34	O/G	23,442	13,416	21,206	1,893	111
Double Bayou	38	O/G	1,546	6,820	409	480	21
Double Bayou, S	65	Oil	2,764	2,134	2,408	1	34
Double Bayou, W	67	Gas	1,338	7,547	80	0	0
East Bay	58	Gas	1,771	9,739	148	0	0
Fishers Reef	31	O/G	24,827	53,305	15,943	3,048	137
Fishers Reef, NE	61	O/G	1,182	4,335	459	0	0
Fishers Reef, S	58	O/G	1,530	4,413	794	2	6
Franks	53	O/G	13,181	8,112	11,829	943	143
Gillock	36	O/G	67,698	7,916	66,379	593	364
Gillock, S	48	O/G	56,740	68,018	45,404	10,796	183
Half Moon Shoal	76	O/G	3,234	12,555	1,141	109	2
Halls Bayou	43	Gas	1,879	8,717	425	47	4
Hannah Island	77	O/G	1,340	6,581	243	209	6
Hitchcock, NE	57	Gas	19,807	87,264	5,263	508	23
Jackson Pasture	43	Oil	1,076	81	1,062	23	51
Jackson Pasture, E	51	O/G	2,133	7,878	820	15	13
Lake Stephenson	61	Gas	5,213	26,871	734	20	1
Martin Ranch	73	Gas	5,172	29,880	192	204	2
Mayes	44	Oil	1,447	111	1,428	17	5
Mayes, S	46	O/G	7,008	30,990	1,843	944	32
Oyster Bayou	41	O/G	138,755	22,909	134,937	2,042	1,040
Point Bolivar, N	71	Gas	57,554	341,407	653	3,616	20
Redfish Reef	40	O/G	59,633	211,129	24,445	4,966	212
Redfish Reef, N	56	O/G	3,300	6,752	2,175	373	37
Redfish Reef, S	59	O/G	10,569	36,463	4,492	908	8
Redfish Reef, SW	57	O/G	19,561	87,799	4,928	1,432	17
Robinson Lake	52	Gas	2,918	16,950	93	475	22
Sarah White	58	O/G	2,719	6,085	1,705	201	7
Sarah White, E	59	Gas	3,432	15,989	767	0	0

PLAY IX continued on next page

APPENDIX B (cont.)

Hydrocarbon Field	Discovery Date	Prod. Type	Total (Mboe)	Gas (MMcf)	Oil (Mbbl)	Gas (MMcf)	Oil (Mbbl)
PLAY IX 9 (cont.)							
Seabreeze	35	O/G	11,791	22,796	7,992	1,759	29
Shipwreck	76	Gas	25,034	145,849	726	364	2
Smith Point	44	O/G	13,061	34,011	7,392	0	0
Smith Point, E	57	O/G	7,875	33,715	2,256	794	43
Stephenson Point	63	O/G	4,505	21,310	953	984	5
Texas City Dike	75	Gas	12,828	69,986	1,164	933	10
Texas City Dike, N	76	Gas	4,269	22,915	450	0	0
Umbrella Point	57	O/G	32,411	98,112	16,059	762	278
White's Lake	44	Gas	1,683	9,062	173	0	0
Willow Slough	37	O/G	5,954	14,694	3,505	1,716	61
Total Play IX Prod.	--	O&G	714,808	1,859,471	404,893	49,804	3,209
PLAY Xa							
Amelia	36	O/G	4,043	17,999	1,043	0	0
Big Hill	49	Gas	5,147	30,712	28	0	0
Big Hill, W	53	Gas	4,037	24,215	1	270	1
Gum Island, N	71	Gas	10,175	40,641	3,401	7,220	637
Hildebrandt Bayou	66	O/G	4,548	18,886	1,400	56	2
Marrs McLean	56	O/G	17,367	97,216	1,164	124	3
Phelan	54	O/G	1,934	5,992	935	0	0
Port Acres	57	O/G	57,661	279,024	11,157	136	130
Port Arthur	59	Gas	11,994	56,764	2,533	0	0
Port Neches	50	Gas	2,716	15,932	61	0	0
Port Neches, N	46	O/G	66,376	369,432	4,804	421	4
Rose City, N	50	Oil	2,840	8,843	1,366	1,318	189
Rose City, S	50	Oil	13,520	1,045	13,346	45	257
Stowell	45	Gas	5,490	32,941	0	0	0
Total Play Xa Prod.	--	O&G	207,848	999,642	41,239	9,590	1,223
Total Production	--	0&G	1,772,418	6,544,029	680,850	148,112	6,242

APPENDIX C. Distal Frio hydrocarbon fields shown in plate 5.

Hydrocarbon Field	Discovery Date	Plate 5 ID No.
PLAY I		
Block 978-S	69	292
Calandria	52	306
Laguna Madre	54	304
Mesquite Rincon	58	303
Murdock Pass	52	299
Murdock Pass, E	64	297
Murdock Pass, N	68	294
Mustang Isl. Blk. 881-L8	83	295
Nile	67	309
Penascal	52	298
Potrero Lopena	52	300
Potrero Lopena, S	66	301
Potrero Lopena, SW	77	302
San Jose	62	305
San Jose, S	79	307
Sprint	54	291
Sprint, S	68	293
Tenerias	53	308
Willamar, SE	53	311
Willamar, SW	73	312
Willamar, W	41	310
PLAY V		
Appling, SE	59	144
Aransas Pass	36	224
Aransas Pass, E	54	215
Baer Ranch	65	134
Bartell Pass	70	191
Bina	76	284
Bina, NE	82	285
Bird Island	38	286
Bird Island, SW	61	288
Blackjack	51	176
Blind Pass	52	218
Burgentine Lake	66	175
Burgentine Lake, SW	67	177
Buttermilk Slough	39	142
Camp Hulen	78	141
Camp Hulen, W	79	140
Cane Island	64	135
Caney	59	128
Cayo del Oso	53	273
Chevron	54	290
Collegeport, N	55	136
Copano Bay, S	62	202
Copano Bay, SW	67	203

APPENDIX C. (cont.)

Hydrocarbon Field	Discovery Date	Plate 5 ID No.
Corpus Channel	53	252
Corpus Channel, NW	56	251
Corpus Christi, E	53	250
Corpus Christi Bay, W	61	258
Crane Island, S	80	271
Dimmits Island	71	262
Dunham Bay	80	183
Dunn-McCampbell	61	287
Encinal Channel	65	259
Encinal Channel, SE	67	261
Enos Cooper	53	238
Estes Cove	68	210
Flour Bluff	36	269
Flour Bluff, E	40	270
Flour Bluff, SE	78	274
Four Corners	77	122
Fulton Beach	47	185
Fulton Beach, E	52	198
Fulton Beach, N	53	184
Fulton Beach, NE	67	187
Fulton Beach, NW	67	188
Fulton Beach, SW	69	196
Fulton Beach, W	51	192
Geronimo	58	234
Geronimo, SE	75	235
Ginny, E	65	214
Goose Island	53	189
Goose Island, S	79	190
Gregory, E	60	237
Gregory, N	53	243
Gwynn	71	278
Half Moon Reef	57	193
Harbor Island, S	81	230
Harrison	83	138
Harvey	50	231
Harvey, E	71	232
Hawkinsville, N	77	123
Headquarters	56	171
Indian Point	56	156
John Welder	60	152
La Quinta	66	249
La Quinta Channel	75	246
La Salle Ranch	80	153
Laguna Larga	49	283
Lamar	29	186
Long Mott, S	51	149
Magnolia Beach	50	147
Magnolia Beach, E	78	146
Mag. Beach-Kellers Bay	52	145
McCampbell	69	233

APPENDIX C. (cont.)

Hydrocarbon Field	Discovery Date	Plate 5 ID No.
Mesquite Bay	74	180
Mosquito Point	67	159
Mosquito Point, E	67	157
Mosquito Point, NE	74	151
Mud Island	64	217
Mudflats	49	212
Mudflats, S	66	213
Mustang Island	49	254
Mustang Island, W	66	260
Nettle	77	170
Nine Mile Point	65	199
Nine Mile Point, E	81	200
Nine Mile Point, W	77	201
Nuarc	66	226
Nuarc, W	79	225
Ocker	64	173
Oso Creek	74	277
Oso Deep	68	276
Padre, N	72	280
Palacios	37	137
Panther Reef	57	161
Panther Reef, E	84	158
Panther Reef, N	64	160
Panther Reef, NW	61	164
Panther Reef, SW	64	169
Panther Reef, W	78	165
Petrucha	62	133
Pita Island	64	279
Portland, E	79	245
Portland, W	56	248
Powderhorn, SW	79	148
Puerto Bay	53	223
Puerto Bay, W	55	222
Quail	67	289
Ransom Island	53	239
Rattlesnake Point	68	211
Redfish Bay	50	247
Redfish Bay, N	59	240
Redfish Bay, NE	59	241
Rockport	80	205
Rockport, S	68	206
Rockport, W	54	204
Rugeley, N	81	124
Rugeley, SW	77	127
Saint Charles	41	179
Saint Charles, N	52	178
Saint Charles Bay, S	66	194
Salt Lake	48	197

APPENDIX C. (cont.)

Hydrocarbon Field	Discovery Date	Plate 5 ID No.
Sam Wilson	54	174
Seadrift	50	150
Shepherd Mott, N	36	126
Silver Lake, W	61	143
South Bay	76	228
Stedman Island	51	229
Stedman Island, W	78	227
Sweeney	58	121
Talley Island	79	209
Talley Island, E	80	208
Torian	80	236
Traylor Island	79	216
Tri Channel	68	253
Turtle Creek	82	139
Virginia	50	182
Wadworth	51	130
Wadworth, S	61	131
Wadworth, W	65	132
Webb Point	66	162
Zoller	53	167
Zoller, E	60	163
Zoller, N	68	166
Zoller, S	63	168
PLAY Va		
Block 749	74	242
Block 772	81	257
Block 774	81	265
Block 794-L	82	268
Block 797-L	83	272
Block 818-L	84	282
Block 901	75	266
Block 926-S	81	275
Clear, S	83	221
Clear, W	83	220
GOM-ST-773-L	67	263
GOM-ST-904	57	267
Mustang Isl. Blk. 773-L	82	264
Mustang Isl. Blk. 883	73	255
Mustang Isl. Blk. 889	55	256
Mustang Isl. Blk. 915-S	85	296
St. Joseph Island	66	219
Samedan	79	281
PLAY VIII		
Austin College	76	117
Clemens, N	63	118

APPENDIX C. (cont.)

Hydrocarbon Field	Discovery Date	Plate 5 ID No.
Clemens, NE	74	119
Clemens, SW	72	101
Cow Trap	51	120
Hoskins, SW	66	112
Peach Point	48	115
Peach Point, S	76	116
Perry Landing	62	114
Stratton Ridge, SE	67	113
PLAY IX		
Acom	60	35
Alligator Point	62	111
Alta Loma	40	100
Alta Loma, E	57	97
Alta Loma, S	53	102
Alta Loma, SW	69	105
Alta Loma, W	56	96
Angelina	67	33
Bacliff	61	82
Barrow Ranch	81	39
Bayview	75	86
Big Hill, N	49	29
Big Hill, NW	61	28
Caplen, S	75	77
Chimney Bayou	66	41
Chocolate Bayou, S	60	107
Dickinson	34	88
Double Bayou	38	42
Double Bayou, S	65	44
Double Bayou, W	67	43
East Bay	58	66
Fishers Reef	31	52
Fishers Reef, NE	61	47
Fishers Reef, NW	84	55
Fishers Reef, S	58	56
Frankland	58	57
Frankland, S	83	58
Franks	53	94
Galveston Blk. 100-L	80	75
Gillock	36	89
Gillock, S	48	90
Glen Point	67	48
Half Moon Shoal	76	80
Halls Bayou	43	106
Hannah, NW	78	67
Hannah Island	77	73
Hannah Reef	49	68
Hitchcock	59	93
Hitchcock, NE	57	95

APPENDIX C. (cont.)

Hydrocarbon Field	Discovery Date	Plate 5 ID No.
Hitchcock, S	59	99
Jackson Pasture	43	49
Jackson Pasture, E	51	46
Lake Stephenson	61	51
Martin Ranch	73	108
Mayes	44	53
Mayes, E	44	50
Mayes, S	46	54
Oyster Bayou	41	37
Oyster Bayou, N	75	40
Oyster Bayou, NE	79	36
Point Bolivar, N	71	81
Rattlesnake Mound	60	110
Rattlesnake Mound, W	74	109
Redfish Reef	40	70
Redfish Reef, N	56	69
Redfish Reef, S	59	71
Redfish Reef, SW	57	79
Robinson Lake	52	45
Sarah White	58	104
Sarah White, E	59	98
Sarah White, W	59	103
Seabreeze	35	34
Shipchannel	76	78
Shipchannel, S	79	83
Shipwreck	76	74
Smith Point	44	64
Smith Point, E	57	65
Stephenson Point	63	59
Texas City Dike	75	85
Texas City Dike, N	76	84
Umbrella Point	57	60
Umbrella Point, E	63	63
Umbrella Point, SE	78	62
Umbrella Point, W	69	61
Willow Slough	37	38
PLAY Xa		
Amelia	36	10
Amelia, S	60	11
Big Hill	49	31
Big Hill, W	53	32
Bridge City	66	4
China	57	15
China, S	59	16
French Island	79	20
Gilbert Ranch	62	23

APPENDIX C. (cont.)

Hydrocarbon Field	Discovery Date	Plate 5 ID No.
Gilbert Woods	61	26
Gilbert Woods, W	78	25
Golden Triangle	60	7
Gum Island, N	71	21
Gum Island, W	78	22
Hildebrandt Bayou	66	13
Lovell Lake	49	12
M Half Circle	81	24
Marrs McLean	56	27
Oak Island	71	19
Phelan	54	14
Pine Forest	80	1
Port Acres	57	8
Port Arthur	59	9
Port Neches	50	2
Port Neches, N	46	3
Rose City, N	50	5
Rose City, S	50	6
Stowell	45	30
Weed	57	17
Weed, S	62	18

APPENDIX D. Acoustic well logs used in regional porosity analysis.

Well No.*	County or Offshore Area	Operator	Lease or Block
1	Willacy	Samedan	#1 Bomba
2	Kenedy	Kelly Bell	#1 St. Tr. 318
3	N. Padre I.	CNG Producing	#1 St. Tr. 318
4	N. Padre I.	Home	#1 Block 902-L
5	Mustang I.	Samedan	#1 Block 988-S
6	Mustang I.	Union California	#1 Block 859-L
7	Mustang I.	Houston O. & M.	#1 Block 866-L
8	Mustang I.	Samedan	#G-1 Block 818-L
9	Mustang I.	Patrick	#1 Block 774-L
10	Nueces	McMoran	#1 St. Tr. 351
11	Aransas	Amerada	#G-1 St. Tr. 198
12	Matagorda I.	Energy reserves Grp.	#1 Block 825-S
13	Calhoun	Louisiana L. & E.	#1 St. Tr. 157
14	Matagorda	Phillips	#1-A St. Tr. N
15	Brazoria	Dow Chemical	#1 McCarthy et al.
16	Brazoria	Texaco	#2 Hoskins Mound Fee
17	Brazoria	Humble	#1 Vieman
18	Galveston	Mesa	#1 Block 245-L
19	Galveston	Apexco	#1 St. Tr. 118-A
20	Galveston	Exxon	#A-180 St. Tr. 266
21	Chambers	Amerada	#F-2 St. Tr. 55
22	Galveston	Mosbacher	#2 St. Tr. 152
23	Jefferson	Houston O. & M.	#1 Jefferson Co. Airport

*See figure 9 for location of map numbers.